Magnetic Nanoparticles for Cancer Therapy

G.F. Goya*, V. Grazú and M.R. Ibarra

Aragon Institute of Nanoscience (INA), Universidad de Zaragoza, Pedro Cerbuna 12, 50009 Zaragoza, Spain

Abstract: Today, technologies based on magnetic nanoparticles (MNPs) are routinely applied to biological systems with diagnostic or therapeutic purposes. The paradigmatic example is the magnetic resonance imaging (MRI), a technique that uses the magnetic moments of MNPs as a disturbance of the proton resonance to obtain images. Similarly, magnetic fluid hyperthermia (MFH) uses MNPs as heat generators to induce localized cell death. The physical basis of these techniques relies on the interaction with external magnetic fields, and therefore the magnetic moment of the particles has to be maximized for these applications. Targeted drug-delivery based on 'smart' nanoparticles is the next step towards more efficient oncologic therapies, by delivering a minimal dose of drug only to the vicinity of the target. Current improvements in this fields relay on a) particle functionalization with specific ligands for targeting cell membrane receptors and b) loading MNPs onto cells (e.g., dendritic cells, T-cells, macrophages) having an active role in tumor grow. Here we review the current state of research on applications of magnetic carriers for cancer therapy, discussing the advances and drawbacks of both passive and targeted delivery of MNPs. The most promising strategies for targeted delivery of MNPs are analyzed, evaluating the expected impact on clinical MRI and MFH protocols.

Key Words: Nanoparticles, Superparamagnetism, Iron Oxides, Hyperthermia, MRI-Contrast agents, Drug Delivery, Cell Separation.

1. INTRODUCTION

Small particles have been in use for biomedical research and *in vitro* diagnostic protocols during the last fifty years [1]. Polymeric microparticles (specially latex microspheres) obtained as highly monosized assemblies have the advantages of biocompatibility and large reactive surface for biological units. These micro-particles have been adopted by food industry for diagnostics and testing in the production line, such as latex agglutination (LA) for identifying staphylococci, streptococci or *Escherichia coli* (*E. coli*). Clinical uses of polymeric microspheres include immunology diagnostics for malignant proliferative plasma cell disorders (i.e., multiple myeloma); immunodiagnostic assay systems using antibody-charged particles for quantification of immunoglobulin molecules in serum or cerebrospinal fluid, and fluorescent neuronal markers for studying the visual cortex [2-5]. For cancer diagnostics and therapy there are currently a number of techniques based on different types of nanoparticles. Nanotechnological advances are at the bottom of the next paradigm shift in cancer research, diagnostics and therapy by improving direct visualization of malignant cells, targeting at molecular level and safely delivering large amounts of chemotherapeutic agents to desired cells. These techniques should be capable of rapid and sensitive detection of malignant cells at early stages.

Table I. Basic Mechanisms and Types of NPs Used for Different NP-Based Diagnostics and Therapy

Diagnostic/Therapy	Basic Mechanism	Type of NPs	Action of the NPs
MRI	Magnetic disturbance of ^{1}H nuclear spin	Superparamagnetic. Large magnetic moment	Contrast agent
Chemotherapy	Biochemical affinity	Inert. Biocompatible. Surface functionalized	Drug delivery
Chemotherapy	Thermal activation, Time-dependent desorption	High specific surface area Specific chemical binding	Controlled release of drug
Neutron Capture Therapy	Nuclear capture and fission	Large neutron cross section (^{10}B and ^{157}Gd)	Neutron capture
Magnetic Hyperthermia	Electromagnetic absorption	Magnetic. Large magnetic moment	Heating
Photodynamic therapy	Photon emission. Photon internal conversion	Polymeric	Activation of photosensitizers. Production of cytotoxic species

The common feature of all nanoparticle-based cancer therapies is the need of specific NPs for achieving the desired therapeutic effect. However, each diagnostic/therapeutic technique requires a different chemical or physical property of the particles involved, which depends on the specific function played by the NPs in that therapy (e.g., vector, porous receptacle, heating agent, magnetic moment carrier, etc…). Sometimes the particle function is activated using an external agent (magnetic fields, light, radiation, etc…) that interacts with the NPs. Therefore the requirements for NPs as biomedical agents span a broad range of novel materials, synthesis strategies, and research fields (see Table **I**).

Magnetic nanoparticles (MNPs) are one sub-class of this broad cancer-therapy designed NPs. The first therapeutic applications of magnetic devices to humans can be chased back to the 16th century, when Austrian physician Franz Anton Mesmer (1734-1815) developed his theories about magnetic fluids [6]. He sustained the influence of invisible 'universal fluids' on the human body (after the Newtonian ideas of 'aether' associated to gravitational forces and tidal cycles), and proposed his theory of 'animal magnetism' gaining notoriety across Europe. Since then Mesmerism (a therapeutics based mainly on hypnotism) has triggered a sustained flood of both research and 'supernatural' quackery.

Pushed by advances in the synthesis of biocompatible magnetic nanoparticles (MNPs) in a reproducible way, the concept of targeting magnetic nanospheres inside microscopic living organisms regained interest and finally became a reality. Since the size of MNPs is comparable to the DNA or subcellular structures, this field

*Address correspondence to this author at the Instituto de Nanociencia de Aragón, Universidad de Zaragoza, Pedro Cerbuna 12, Zaragoza 50009 Spain; Tel: (+34) 976 76 27 83; Fax: (+34) 976 76 27 76; E-mail: goya@unizar.es

1573-4137/08 $55.00+.00

opened the door for cell separation strategies using magnets as external driving forces. Similarly, recent advancements on binding chemistry of biological units onto MNPs surface and the engineering of particle's surface/shape have opened new exciting possibilities for drug delivery with high selective vectors. Nonetheless, *in vivo* applications entangle subtle problems related to the response of a living organism to alien objects (i.e., NPs-drug assemblies). For example, even if a perfectly selective drug delivery system could be designed (e.g., by using some monoclonal antibody-loaded particles), any real experiment has to overcome the problem of immunological reactions triggered by the invading NPs within the host, mainly from the reticuloendothelial system (RES).

At present, most applications of MNPs are based on the following physical principles:

a. The application of controlled magnetic field gradients (i.e., a magnetic force) around the desired target location for remotely positioning MNPs in organs or tissues (targeting, magnetic implants, magnetic separation applied to the sequencing of DNA, etc… Sec. 3.2);

b. The utilization of the magnetic moment of the MNPs as a disturbance of the proton nuclear resonance (e.g., contrast media for Magnetic Resonance Imaging, MRI, Sec. 3.3).

c. The magnetic losses of nanometric particles in colloids for heating purposes (magnetic hyperthermia Sec. 3.4.).

Any of the above applications requires the concourse from many disciplines in order to solve wide-ranging biomedical problems, and there are great efforts being done to approach these problems within multidisciplinary teams. The outcome of these efforts is reflected in comprehensive works and reviews on biomedical applications of MNPs [7, 8, 9,10]. In this work we propose to review the most recent developments of MNPs applications to cancer therapies, with special emphasis in the physics behind new approaches. In addition to a state-of-the-art landscape of the field, we identify the main obstacles yet to be solved for the next generation of MNPs and their applications.

2. BASIC CONCEPTS

The underlying physics of biomedical applications of magnetic nanoparticles include several concepts from electromagnetic radiation, solid state magnetism, surface chemistry and fluid rheology. Thus, a brief review of the main concepts at a basic level is included in this section in order to provide the basic language from these areas.

2.1. Electromagnetic Radiation

Electromagnetic (EM) radiation is a fundamental tool in cancer therapy, extensively used for both diagnostics and therapy. Physical interactions between EM waves and living matter can be very different depending on the portion of the electromagnetic spectrum considered. A variety of clinical tools have been established in physical medicine based on direct emission and detection of EM waves such as x-ray radiography, computer tomography scanning (CT scan) and gamma-ray radiotherapy from radioactive isotopes. Many other techniques rely on indirect uses of EM radiation such as positron-emission tomography (PET), magnetic resonance imaging (MRI), and microwave hyperthermia (MWH).

Fig. (**1**) schematizes the different ranges of the EM spectrum used by different techniques, and also puts comparatively some physical and biological phenomena occurring within each region. The importance of this "EM landscape" is connected to absorption of energy by biological units, since the shorter the wavelength, the higher the energy content. Organic materials composed of long-chained molecules with C-C (or C=C) backbones and other carbon bonds like C-H, C-N, can absorb EM radiation at some specific frequencies that are, consequently, biologically dangerous. As an example, covalent bonds can be broken at approximately 10^{12} Hz ($\lambda \approx 300$ nm, in the UV range) [11]. Larger units have more complex (secondary, tertiary) structures, and may be bound to other units by entanglement alone, secondary forces or chemical bonds. Due to this variety of binding forces, living matter displays several 'frequency windows' where interaction with EM radiation can destroy biological units and/or metabolic functions. The frequency ranges employed by the techniques of Fig. (**1**) are usually grouped in two coarse classes: those based on non-ionizing radiation (basically radiofrequency and microwaves), and those using ionizing radiation (high-energy X-rays and gamma-rays). The limit between these areas is defined by the energy threshold to break C-C, C-H and C-N covalent bonds, which would imply the breaking of fundamental organic molecules as DNA, RNA, proteins, etc…

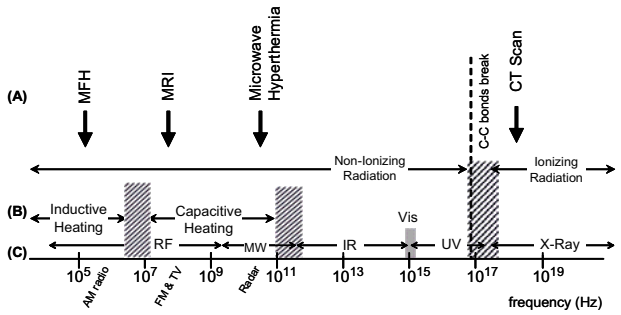

Fig. (1). (A). Frequency ranges for some of the most used diagnostic/therapy equipments (MFH = Magnetic Fluid Hyperthermia, MRI = Magnetic Resonance Imaging). (B). The respective main physical mechanisms at each frequency range. Also shown in (C) is the common nomenclature for the electromagnetic waves at each region: RF = radiofrequency; MW = microwaves; IR = infrared; Vis = visible; UV = ultraviolet and X-

In this review we will restrict our discussion only to those techniques that use non-ionizing radiation, i.e., the low-frequency phenomena exploited by MRI and hyperthermia.

2.2. The Novel Tool: Nanomaterials

Magnetic nanoparticles can be produced by a number of physical and chemical routes that differ in the final properties of the products. A broad classification scheme can be made based on the physical state of the starting materials as follows. In the ***top-down*** strategy, the starting bulk material is reduced to nanometric scale in one (thin films), two (nanowires) or three (nanoparticles, or quantum dots) dimensions. This route is based often in physical processes like mechanical alloying, laser machining, laser chemical etching, reactive ion etching, etc… On the contrary, the ***bottom-up*** approach uses atomic or molecular units as starting materials to grow larger, nanometric structures. Bottom up techniques include chemical vapor deposition (CVD), reactive sputtering, plasma enhanced CVD, pulsed laser deposition (PLD), molecular beam epitaxy (MBE), and also wet routes like sol-gel and microemulsion techniques. Most of the above techniques have attained good control of the physical parameter of the products such as phase purity, particle shape, crystalline order and the attainable range of particle sizes, although tailoring all these parameters in a single sample remains a challenging task. The need of higher densities in magnetic recording media for hard disk drives along the last decade boosted the development of new synthesis routes for NPs and a deeper understanding of the associated new physics at the nanoscale [12]. Similarly, the current advancement in nanomagnetism has opened the way to applications for tagging and imaging biological units of comparable (and larger) dimensions.

Only in recent years the synthesis of free (i.e., without solid substrates) magnetic nanoparticles with controlled sizes (within the ca. 1 to 100 nanometers) was attained in reproducible ways. A large number of works have been reported on synthesis of NPs by physical methods like laser ablation [13], ball milling [14], molecular beam epitaxy (MBE) [15], sputtering [16], arc discharge [17] or laser pyrolysis [18]. Chemical routes commonly used include co-precipitation [19], impregnation [20], and molecular-based sol–gel process [21]. Recently, the synthesis of iron NPs displaying high magnetic response was achieved through a single-step arc-discharge method [17]. The structure of the resulting particles (shown in Fig. (**2**) consists of a Fe-rich core and SiO_2-rich surface, which are appealing for biomedical applications because their silica surface that could allow direct functionalization.

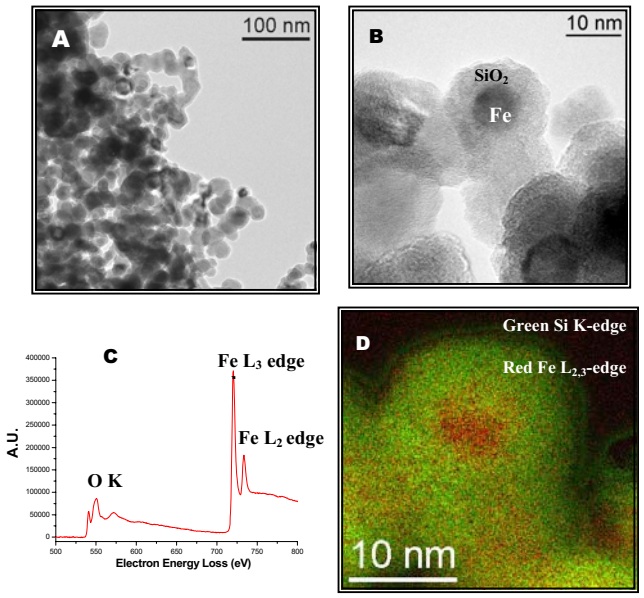

Fig. (2). (A), (B) Transmission electron (TEM) images of the silica-coated iron nanoparticles (C) Electron energy loss spectra (EELS) showing the presence of metallic iron. (D) EFTEM shows an iron-rich core and a silica-rich shell. Reprinted with permission from ref. [17].

Applications of MNPs on biomedical areas require the use of a *colloidal ferrofluid*, or *magnetic colloids* [22], which consist of a suspension of magnetic particles of nanometric sizes in a carrier liquid like water. These colloids usually have particle concentrations in the range of 10^{21}-10^{23} particles/m^3. The stability of any magnetic colloid depends on the balance between attractive (van der Waals and dipole-dipole) and repulsive (steric and electrostatic) forces between the particles and the supporting liquid [23]. Temperature is also a relevant parameter for stability due to energy transfer from the molecules in the liquid carrier (Brownian motion) to the nanometric particles. Therefore, to stabilize the suspended MNPs against these forces they are often coated with a shell of an appropriate material. Nanoparticles stabilized by electrically neutral molecules (amphiphilic molecules, as oleic acid or alkylsilanes) constitute a *surfacted colloid.* Steric repulsion between particles acts as a physical barrier that keeps grains in the solution and stabilizes the colloid.

For some industrial applications nonpolar media such as oil or organic cosolvents are preferred, and therefore the surfactant is needed to form an external hydrophobic layer. The polar head of the surfactant is attached to the surface of the particles and the hydrophobic tail is in contact with the fluid carrier. For particles dispersed in a polar medium, as water, a double surfactation of the particles is needed to form a hydrophilic layer around them. The polar heads of surfactant molecules can be cationic, anionic, zwitterionic or nonionic.

Also for *in vivo* applications the stability of the magnetic colloid must be granted in order to avoid embolism from agglomerates within arteries, thus in these cases biocompatibility is an additional requirement for the surfactant. A number of biocompatible surfactants have been used including dextran, polyethylene glycol, citric/aspartic acids, and more complex molecules like peptides and protein shells [10]. Further requirements for the particle cores composing a biomedical colloid are to have low toxicity levels as well as a large saturation magnetic moment, in order to minimize the required clinical doses. Magnetite (Fe_3O_4) have shown to fulfill the requirements of high Curie temperature (T_C), high saturation magnetic moment (M_S ~ 90-98 emu/g, or ~450-500 emu/cm^3), and the lowest toxicity levels yet known in pre-clinical tests [24]. Although from the production point of view the material is cheap and relatively easy to obtain in high purity form, the manufacture of MNPs of few magnetic manometers structurally and magnetically ordered is a big challenge because the high surface/volume ratio causes the effects of superficial disorder to be dominant.

2.3. The Driving Force: Nanomagnetism

The magnetism of a solid is originated from the contributions of the electrons constituting a solid. The quantum properties of electrons that determines the magnetic behavior of a solid are a) the *spin angular moment*, ***s***, taken from the classic analogue of a sphere rotating about it own axis, and b) their *orbital angular moment* ***l***, since electrons also carry electric charge so that 'moving around' in quantum orbits also contributes to the magnetic moment. These electrons also determine the strength of the interaction between atoms in a solid, making the basis of the different macroscopic behavior observed in nature. At macroscopic scales, these magnetic interactions between atoms, together with the crystalline structure of the solid, originate the magnetic response of materials. When the magnetic interactions are weak, the thermal agitation at room temperature can make the magnetic moments to flip over continuously, so that the average magnetic moment measured is very small or zero.

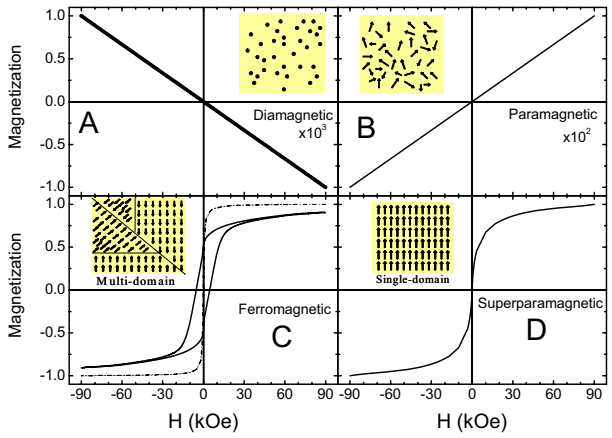

Fig. (3). Different magnetic materials display dissimilar performances: a) diamagnetic atoms in solids have negligible magnetic moments (represented as black dots); b) in paramagnetic solids magnetic atoms are not ordered because of thermal energy that shakes each atom randomly; c) In a ferromagnetic material, displacement of the domain walls (DW, schematically shown in the inset) result in open hysteresis cycles. d) For single domain particles there are no DW, so that in the SPM state the whole magnetic moment of each particle is shook in the same way as in the paramagnetic material (b).

These materials are broadly called non-magnetic, and display a linear response to the applied field, as shown in Fig. (**3a**) and **b**). For stronger magnetic interactions, the atoms within the solid can align the atomic magnetic moments parallel (ferromagnet) or anti-parallel (antiferromagnet) configurations. The former configuration result in very dissimilar magnetic behavior, shown in Fig. (**3c**), whereas in the antiferromagnet the antiparallel alignment can reduce the total moment to zero, yielding a behavior similar to a paramagnet Fig. (**3b**).

Although a ferromagnetic material should have *all* its magnetic moments pointing in the same direction, a macroscopic piece of material cannot have this configuration because the amount of magnetostatic energy stored should be huge. The way in which a solid can reduce this otherwise huge magnetostatic energy is to break itself up into regions called *magnetic domains*. Within a single domain all magnetic moments remain parallel, but each domain is randomly oriented so that the net magnetic moment of the sample is nearly cancelled. (See Fig. **3c**.). This situation generates interfaces between domains called domain walls (DWs), where adjacent magnetic moments are in a non-favorable configuration, so that these domain walls are highly energetic. Even though some energy is stored inside domain walls, the overall decrease in the total magnetic energy favors the multi-domain configuration. Being formed by a competition between magnetostatic and exchange energies, domain walls have a finite width, δ, determined by the ratio between these energies [25].

Domain walls can move in response to an applied field: creation, growth and extinction of domains can be induced by an external magnetic field, because the external field imposes a preferred direction for the magnetic moments. For the spins in a given domain to change their orientation it is required that the walls of that domain will displace. This is known as Barkhausen effect, and is an irreversible process in the sense that the pinning and displacement of DWs depends of structural imperfections of the atomic arrangements (defects, dislocations, vacancies, etc…). However, the magnetic field required to eliminate all DWs (i.e., to align all magnetic moments in the same direction) has a definite value for a given sample, and is very reproducible. The two ways of visualizing the Barkhausen process (i.e., domain wall displacement or domain growth) are equivalent and so are used.

When the volume of a small particle is reduced below a certain value, called critical domain size, $D_{Critical}$, the proximity of many domain walls in a small volume is not energetically stable, so that a single-domain configuration is adopted Fig. (**4**). Within this single magnetic domain all the atomic magnetic moments will be magnetized along the same direction, adding up so they behave like a giant magnetic moment (superparamagnet). This situation was first envisaged by Frenkel and Dorfman [26] and further developed by Kittel [27] by calculating the magnetic and anisotropy energies of various domain configurations for thin films, particles, and needles of ferromagnetic material. The value of critical size $D_{Critical}$ below which a particle of a given material becomes single-domain is determined by intrinsic properties of that material (e.g., magnetic anisotropy, magnetic moment and exchange anisotropy), and also on the particle shape. Calculations for metallic Fe using this simple model yield values of $\delta \approx 30$ nm, in fair agreement with the critical size found in iron-NPs. But even for assumed spherical particles, large differences between magnetic materials are reflected in a broad range of critical sizes, as shown in Table **II**.

In spite of this huge magnetic moment of single domain particles, their interaction is weak, so like in a paramagnet the thermal energy forces the magnetic moments to rapidly flip over. The reversion mechanism is characterized by the probability of switching the particle's magnetic moment μ among different spatial orientations or, in terms of the Néel model [28], the relaxation time τ. Being a thermally activated process, the relaxation time of μ is described by the Néel-Arrhenius law

$$\tau = \tau_0 \exp\left[\frac{E_a}{k_B T}\right] \qquad \textbf{(I)}$$

where $E_a = K_{eff} V$ is the energy barrier that separates two energy minima between magnetization states (up and down), k_B is the Boltzmann constant, and τ_0 is the pre-exponential factor related to an attempt time, of the order of 10^{-9} - 10^{-12} s [25]. Therefore if the magnetization of a single-domain particle is to be measured, the experimental measuring time window τ_M should be smaller than the value of τ for a given temperature and E_a value. If $\tau_M >> \tau$ the fast relaxation of the magnetic moments due to thermal energy makes the system to behave as a (super)paramagnet.

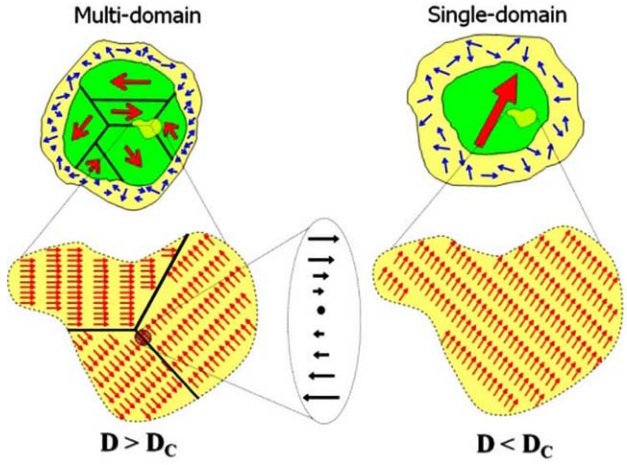

Fig. (4). Left: schematic view of magnetic domains in a multidomain ferromagnetic particle having size larger than the critical diameter $D > D_C$. For this particle the whole material breaks down into randomly oriented magnetic regions. At the interface between domains, magnetic moments are twisted to fit the orientation at both sides of the domain walls. Right: for $D < D_C$ the material becomes a single-domain particle. The spin disorder at the particle surfaces are represented by a annular region in both cases.

The passage from the 'blocked' to the fast-flipping state is called superparamagnetic transition, and for a given particle volume *V* it will occur at a temperature T_B satisfying eq. (I)

$$T_B = \frac{K_{eff} V}{k_B \ln\left(\tau_M \tau_0\right)} \qquad \textbf{(II)}$$

that shows how the blocking temperature T_B depends on the measuring time window, τ_M, of each experimental technique. A wide range of time windows that can be explored by a proper choose of the experimental technique. For example, a typical dc magnetization measurement spans an experimental time τ_M of ~10^2 s; for Mössbauer spectroscopy the measuring time depends on the Larmor precession time τ_L of the nuclear magnetic moments, i.e., $\tau_M \approx \tau_L$ where $\tau_L = 10^{-8}$-10^{-9} s in the case of ^{57}Fe nuclei, and for neutron scattering measurements the experimental time τ_M is ~10^{-12} s. As the transition temperature T_B is observed when $\tau \sim \tau_M$, the blocking temperatures observed can differ in orders of magnitude depending on the experimental technique used. The above ideas show that the concept of superparamagnetic (SPM) state it *is not* an intrinsic characteristic of a given material, but depends on the measuring conditions. If results from different experiments are to be compared, reporting a T_B value should be accompanied by the proper experimental information.

Table II. Values of Saturation Magnetization M_S and Single-Domain Critical Sizes $D_{Critical}$ for Different Magnetic Materials. Values at Room Temperature

Material	M_S (emu/g) †	$D_{Critical}$ (nm) ††
Iron (α-Fe)	217.9	7 - 11 nm
Nickel	57.5	~ 110 nm
Cobalt	162.7	~ 60 nm
Magnetite Fe_3O_4	91.6	~ 20 – 30 nm
$CoFe_2O_4$	80.8	40 nm
Hematite α-Fe_2O_3	~ 1	13 nm
NdFeB	171	~ 300 nm
$SmCo_5$	164	750 nm
$BaFe_{12}O_{19}$	72.0	900 nm

(† values at room temperature. †† For spherical shape)

Above the blocking temperature, T_B, the contribution from an ensemble of SPM particles to the magnetization M(H,T) is described by the Langevin relation

$$M(H,T) = N\mu L\left(\frac{\mu H}{k_B T}\right) = N\mu\left[\coth\left(\frac{\mu H}{k_B T}\right) - \frac{k_B T}{\mu H}\right] \quad \textbf{(III)}$$

where $M_S = N\mu$ is the saturation magnetization due to N particles with magnetic moment μ, and *L(x)* is the Langevin function of argument $x = \mu H/k_B T$ i.e., the ratio of magnetic to thermal energy. This expression assumes that the system is composed of *noninteracting* and *monodisperse* particles. However, real systems do have a distribution of particle sizes, and quite often the analysis of particle size distribution by photon correlation or TEM microscopy results in a distribution profile similar to the log-normal distribution

$$f(d) = \frac{1}{\sqrt{2\pi}\,\sigma d}\ \exp\left(-\frac{\ln^2(d/d_0)}{2\sigma^2}\right) \quad \textbf{(IV)}$$

where σ is the distribution width and d_0 is the median of the distribution. Theoretical grounds have been given for the use of this distribution shape to model crystal growth in supersaturated solutions [29], and its use has been extensively used for nanostructured systems because it inherently represents positive (and skewed) particle size populations.

Therefore calculations of the magnetization M(H,T) for any real system can be improved by using the log-normal distribution for μ values,

$$f(\mu) = \frac{1}{\sqrt{2\pi}\,\sigma\mu}\ \exp\left(-\frac{\ln^2(\mu/\mu_0)}{2\sigma^2}\right) \quad \textbf{(V)}$$

where $f(\mu)$ is the magnetic moment distribution. Including eq. V into eq. III, the magnetization of an ensemble of NPs with size distribution can be expressed as a weighted sum of Langevin functions [30]

$$M = M_S^{bulk}\int_0^\infty \mathrm{L}\left(\frac{\mu H}{k_B T}\right) f(\mu)\,d\mu \quad \textbf{(VI)}$$

In this expression, M_S^{bulk} is taken as the bulk saturation magnetization of the material, which is assumed temperature-independent (this approximation works well for $T_B << T << T_C$), and the magnetic moment μ of each particle is related to the particle volume *v* by the product $\mu = vM_S$, so that the distribution of particle sizes will be reflected in a distribution of magnetic moments. The weight function $f(\mu)$ is a probability density, relating μ_0 to the most probable magnetic moment (μ_{max}) by

$$\mu_{max} = \mu_0 \exp(-\sigma^2),$$

i.e., μ_{max} corresponds to the maximum of $f(\mu)$. The average (mean) magnetic moment (μ_m) is in turn related to μ_0 by

$$\mu_m = \mu_0 \exp\left(\frac{\sigma^2}{2}\right).$$

To extract the particle size from the above fits, a specific geometry (usually spherical) must be assumed. For spherical shape the magnetic fitting parameters are related to the corresponding volumetric parameters through the simple relations [31]

$$\mu_0 = M_S\frac{\pi}{6}d_0^3$$

$$\langle d\rangle = d_0\exp(\frac{\sigma_d^2}{2})$$

$$\sigma_\mu = 3\sigma_d$$

so that the median and average particle diameters can be obtained from the magnetic measurements.

2.4. Heat Generation

The study of heat generation under ac fields has been historically related to electrical machines, seeking to minimize power losses to improve the performance of electro-mechanic conversion devices (motors, transformers, etc…). The simulation and measurement of magnetic losses in magnetic materials (mostly iron and its alloys NiFe and SiFe) have been developed along the last years for high-performance electromechanical devices subjected to adverse working conditions of high frequencies and harmonics contents. Power losses in these materials are considered as the sum of two components, $P_T = P_F + P_H$, where P_T are the losses due to eddy (Foucault) currents and P_H are the hysteretic losses, related to domain creation, propagation and extinction inside the material. Equations for eddy currents are solved by conventional electromagnetic theory. However, hysteresis loss has a nonlinear behavior:

$$P_H = f^n k_H B_P^{\phi} \quad \textbf{(VII)}$$

where f is the frequency in Hz, B_P is the peak induction and k_H, n and ϕ are adjustable parameters depending of each type of material. This empirical expression proposed by Steinmetz more than 100 years ago is sill used for manufacturers to estimate the hysteretic losses at the induction values of the machine's operating regime [32].

The search for new materials with better performance yielded the incorporation of nanostructured composites into the magnetic core of AC motors and transformers, resulting in a better understanding of the microscopic mechanisms involved in magnetic losses of nanostructured phases [33].

Unfortunately, the situation regarding power losses in MNPs for biological applications is quite different from the described above: systematic studies on the mechanisms of power losses in magnetic colloids are rather scarce, and a systematic body of measurements in MNPs under physiological conditions is still lacking.

For a piece of metal subjected to low- and medium-frequency alternating fields (> 10^2 – 10^3 Hz, for example the case of nuclei of electrical motors) the main mechanism of power losses is parasitic currents (eddy currents). On the other hand, in ceramic materials the dissipation of power is mainly originated in processes of nucleation, growth and extinction of magnetic domains. For single-domain particles in physiological conditions the situation differs radically, because a) the magnetic saturation is reached by coherent rotation of the total magnetic moment of each particle; and b) the hysteresis cycles are theoretically reversible and thus they do not entail magnetic losses. In addition to coherent rotation to be considered for single-domain particles, physiological conditions allow mechanical rotation of the particles as a response to the external magnetic field, at least for low frequencies [23]. It follows that for colloidal dispersions the analysis of the heat transference processes must include the effects of both the Brownian motion and fluid. For biomedical applications based on the increase of temperature as magnetic fluid hyperthermia (MFH) therapy, it is clear that the mechanisms of power losses in colloids must be identified before new, more efficient therapeutic materials can be designed to *maximize* the generation of heat.

Once the heat is generated at the magnetic particles, the problem of heat propagation in living matter becomes an important one. Originally, the heat flux propagated in non-homogeneous materials such as biological tissues have been studied in meat-containing food products [34,35]. In these models the thermal propagation wave is described using an hyperbolic heat transfer model [36], characterized by a thermal relaxation time, of the order of 20–30s, and a differential equation governing the propagation speed of the heat flux, q, given by

$$q = -\tau \frac{\partial q}{\partial t} - k_t \nabla T \quad \textbf{(VIII)}$$

where τ and k_t are the thermal relaxation time and thermal conductivity, respectively. Applying the above model to real situations of living organisms requires the inclusion of the system's response to local heating, mainly blood perfusion that acts as an efficient refrigerating system in highly vascularised tumors. This is done by using Pennes' equation to estimate the temperature field T(x,y,z,t) at nearby tissues [37]

$$\frac{\partial T}{\partial t} = \frac{1}{\rho_t C_t}\left\{k_t \nabla^2 T - w_b c_b (T - T_a) + Q\right\} \quad \textbf{(IX)}$$

where ρ_t and C_t are the density and the specific heat capacity of the tissue, respectively, Q is the density of heat production rate, T_a is the temperature at infinite distances, and w_b, c_b are the perfusion rate and specific heat capacity of blood, respectively. Given all the relevant physical parameters and eq. IX, the heat distribution in any internal element of the body could be calculated by solving the inverse heat transfer problem. However, the complex boundary conditions associated to internal organs is the major obstacle for the use of this model. Nevertheless, heat generating diagnostic tools such as high intensity focused ultrasound (HIFU) and MRI have used this approach with some success to evaluate potential hazards and to establish tolerance limits for clinical protocols [38,39]. A complementary approach has been reported by Andrä *et al.* who made numerical simulations of the spatial temperature distribution during exposure to ac magnetic fields with the physical parameters close to the experimental clinical situation for breast carcinoma, and compared the results with *in vitro* experiments [40].

The heating capacity of a magnetic material or electromagnetic device is quantified through the specific absorption power rate (SAR), defined as the amount of energy converted into heat per time and mass [41]. In terms of the usual experiments and parameters for magnetic colloids, the loss power per gram of Fe_3O_4 is obtained from the heating curves within the initial ΔT temperature rising interval through the definition

$$SAR = C_S \frac{\Delta T}{\Delta t} = \frac{Q}{\rho_t}, \quad \textbf{(X)}$$

where C_S is the sample heat capacity, defined as a mass-weighted mean value for a given concentration of magnetic material, calculated as

$$C_S = \frac{m_{Fe} c_{Fe} + m_l c_l}{m_{Fe} + m_l} \quad \textbf{(XI)}$$

with c_{Fe}, m_{Fe} and c_l, m_l being the specific heat capacities and masses of magnetic material and liquid carrier, respectively. The last member shows the relationship between the functional definition of SAR and eq. IX.

From the instrumental point of view, there is a need of innovative equipments for measuring the many phenomena involved in power losses in fluidic samples, as discussed in Sec. 3.4.a.). For example, measuring the SAR of a biocompatible colloid under physiological conditions requires generating RF waves with variable frequencies and applied fields, mounted around an appropriate Dewar to keep the experiment adiabatic, with the corresponding calorimetric measuring system.

3. APPLICATIONS OF MAGNETIC NANOPARTICLES

3.1. Magnetic Drug Targeting

Most of the pharmaceuticals for anticancer therapy developed up to now are non-specific for the malignant cells to be targeted, so that they spread across the whole body after been injected. Consequently, for attaining the concentration threshold of any anticancer drug at the desired location, the healthy parts of the body are exposed to similar concentration levels. This situation limits the maximum dose of a given drug based on toxicity side-effects criteria. Also, since most drugs are processed and excreted through either the liver or the kidneys, the administration of these drugs to patients with kidney or liver damage may result in unbearable toxicity levels in a patient unable to metabolize and excrete it. Local injection is of course the simplest targeting strategy to solve the above problems, but it is restricted to sizeable tumors and limited by the accessibility to the tumor region. In order to chase metastatic cells in a whole organism, molecular recognition mechanisms must be used.

A promising alternative for cancer treatment relays on the ability of therapeutic agents to selectively reach the desired target after intravenous administration. The concept of nanoparticle-based nanovectors involves a high degree of specificity, which makes these NPs unmatched candidates for the next generation of drug delivery methods. The idea about the next generation of NPs is that they should be able to perform, in addition to their specificity and therapeutic tasks, active processes like monitoring cell status through physical indicators, or specific cell activities by reactive signal emission. These devices, if achieved, will constitute true platforms capable of hosting several components that could actively perform specific tasks of diagnostics and therapeutics functions at the cell scale.

However, several key processes are still to be tailored before molecular specificity levels can be attained, such as

- ✓ the way in which the drug is stored in the NPs;
- ✓ the mechanism that drives the NPs towards the target; and
- ✓ the biological barriers that need to be overcome.

Each of these developments has its own technical challenges and involves different research fields, thus each solution must be considered from specific viewpoints before they can be all integrated onto a single outcome.

Accumulation of high drug concentrations can be achieved in principle because of the surface/volume ratio, R_{sv}, in 5-nm particles can be as high as $R_{sv} = 3.3\ nm^{-1}$ for perfectly spherical shape. Depending on its chemical characteristics, the drug to be stored can be attached to the NPs after proper functionalization of the free surface by using suitable terminal groups, and this is usually performed by physical adsorption incorporation during the production of the acrriers, or by covalent attachment to any reactive surface groups.

The appeal for using nanoparticles in selective tumor targeting is the potential to deliver a concentrate dose of drug in the vicinity of (or even inside) the target tissue, reducing drug exposure of healthy cells. This could be done by means of physical interactions, or passive/active targeting [42].

Physical targeting can be achieved *via* the guidance of superparamagnetic nanoparticles through an external magnetic field. There are several examples that show the successful accumulation of superparamagnetic particles applied intravenously, aimed at specific locations by means of external magnets [43, 44].

Passive targeting takes advantage of the enhanced permeability and retention (EPR) effect of tumor tissues [45]. The EPR effect is a consequence of an incomplete vascular architecture due to the rapid vascularization that is orchestrated by the tumor in order to provide the nutrients that are necessary for its fast expansion. This leaky vasculature allows extravasation of circulating macromolecules as well as small particles within the tumor interstitium, which together with other factors such as poor lymphatic drainage results in drug accumulation [46, 47].

The other way to deliver drugs to any desired target involves the functionalization of the surface of nanoparticles with monoclonal antibodies or ligands to tumor-related receptors, taking advantage of the specific binding ability between an antibody and antigen, or between the ligand and its receptor [48-50]. Within this approach, several differences between cancerous and normal cells can be exploited including: uncontrolled proliferation, insensitivity to negative growth regulation and antigrowth signals, angiogenesis and metastasis [49,51].

It is well known that, for most cancer cells, the grow rate is faster than in normal cells. One mechanism underlying this growth is the overexpression of receptors that allows the uptake of growth factors *via* receptor-mediated endocytosis more efficiently than normal cells [49]. This could be use as a "Trojan horse" to deliver anticancer agents, decorating the surface of nanoparticles with antibodies or ligands that specifically binds to these receptors. An example of a highly selective tumor marker is folate receptor, which is absent from normal tissues or it is inaccessible to circulating drugs due to its apical polarized localization in normal endothelial cells. However, this receptor is fully accessible and over-expressed in many types of cancer cells including ovary, brain, kidney, breast, and lung cancers [52-54]. By this way cancerous cells can efficiently capture folate, a form of water-soluble B vitamin that is needed in order to grow and divide. One of the strategies that were reported to targeting folate receptor-positive tumor cells is based in the ability of folate receptor to endocitose proteins that are covalently bound to it. This strategy has been used by many research groups to show that nanoparticles decorated with folic acid (a high affinity ligand for folate receptors) can be successfully internalized inside tumor cells [55, 56].

Another difference with normal cells that could be exploited to selective target cancerous cells is their acquired ability to avoid apoptosis, defined as a set of programmed cellular processes that result in cell death. One way of avoiding apoptosis in a certain variety of human tumors that includes lung, colon, pancreas, prostate and breast cancer, involves the over expression by malignant cells of a protein that inhibits this process known as survivin. This protein is expressed during embryonic development but is absent in most normal, terminally differentiated tissues. Therefore, survivin could be utilized as a tumor antigen [57, 58]. As there have been developed several antibodies against survivin, immunotherapy could be a conceivable approach to treating survivin-positive tumors [59].

Cancer cells can furthermore trigger sustained angiogenesis. All solid tumors, primary and metastatic, develop the ability to trigger neovascularization in order to provide oxygen and nutrients and remove metabolic wastes. Among the multitude of factors that have been identified as "*angiogenic*," meaning that they are released by tumors as signals for angiogenesis, vascular endothelial growth factor (*VEGF*) has emerged as one of the most important for sustaining tumor growth [60-62]. Therefore considerable efforts are being done to block the VEGF receptor from binding the growth factor by the use of anti-VEGF antibodies, anti-VEGF receptor antibodies and VEGF receptor inhibitors [63, 64]. Functionalization of magnetic carriers with these molecules could open the possibility of imaging angiogenesis and provide the basis for an efficient early-detection technology.

There are a wide variety of methods that could be use to attach a tumor marker biomolecule to the nanoparticle surface [65-67], but often the number of those biologically efficient are reduced to a minimum. The bottom line is that in all cases the biological activity of the biomolecules to be attached must be preserved. This is a most difficult task if the biomolecule in question is asymmetric like an antibody. One way to avoid losing of antigen binding capacity is the technique called site-specific immobilization of antibodies, in which the antigen-binding site (i.e., the two Fab domains) is oriented upward and away from the nanoparticle's surface. Perhaps the most interesting way to accomplish their oriented immobilization reported to date is the covalent attachment *via* the carbohydrate moieties localized on the antibody molecule's Fc region [68, 69].

Of course, functionalizing nanoparticles with tumor markers alone does not grant to reach the targeted cells: when nanoparticles are administered intravenously they adsorb plasma proteins (opsonization process) that make them easily recognizable as "intruder objects" by the immune systems, and cleared by macrophages of the mononuclear phagocytic system (MPS). The typical final biodistribution is approximately 80-90% in the liver (Küpfer cells), 5-8% in the spleen and 1-2% in bone marrow [42,48,70]. Such propensity of MPS for endocytosis/phagocytosis of nanoparticles could be utilized to effectively deliver therapeutic agents in tumors local-

ized in MPS-rich organs/tissues like hepatocarcinoma, hepatic metastasis arising digestive or gynaecological cancers, bronchopulmonary tumors, etc [45,71]. Therefore reaching tumor locations other than the above mentioned requires the nanoparticles to avoid their clearance by the MPS. This has led to the concept of long circulating or "stealth" particles. As result from several investigations, the conclusion widely accepted at present is that the smaller, more neutral and more hydrophilic the nanoparticle surface, the longer its plasma half-life [66,72-74]. Indeed, the use of hydrophilic polymers/surfactants (dextran, PEG, poloxamines, etc) has demonstrated to be an efficient method for coating the surface of several inorganic nanoparticles. These coatings provide a "cloud" of hydrophilic and neutral chains at the particle surface which reduces plasma proteins adsorption [75, 76]. The extended half-lives of inorganic NPs having a hydrophilic macromolecular corona results in measurable concentrations in blood after several hours (up to 24h in rats and 45 h in humans) depending on particles size and the characteristics of the coating polymer [77].

Cancer is a very complex disease, where the cancer cell is only one of the many elements influencing the uncontrolled growth and spread of abnormal tissue. A continuously growing body of evidence suggests that also tumor microenvironment is an important factor in cancer cell growth, invasion and metastatic progression. A lot of work is being done in order to take advantage of the capability of multifunctional design of nanoparticules to address multitarget interaction and by this way to manage this complex interaction to stop growth and spread of cancer [50, 78]. The ultimate objective to be reached is the design and development of multifunctional nanoparticles of the so-called third generation. This generation of NPs will not only allow detecting targeted cells and delivering site-specific cytotoxic drugs, but also to assist in imaging the tumoral environment, and generate a signal reflecting the evolution of treatments. Moreover it will be required that the NPs be able to sense intracellular changes to launch early treatments in order to prevent precancerous cells from becoming malignant. To reach this ambitious goal greater multidisciplinary efforts are required for understanding the subtle mechanisms of biological interactions, as well as further knowledge of particle engineering at the atomic scale.

3.2. Cell Separation

Early technologies to separate biologically important substances were developed more than fifty years ago based on different driving forces. Filtration is perhaps the oldest protocol for cell separation, and yet it remains a key technique in many laboratories and industries due to new developments of synthetic micro- and nano-porous materials. Centrifugation is another classical method based on the application of a centrifugal force[1] to separate biological units from their surrounding medium on either a batch or a continuous-flow basis. Differential centrifugation is based on the size of the particles in differential centrifugation, and is the preferred technique for isolation of cells in clinical applications, whereas the alternative density gradient centrifugation is employed for purification of subcellular organelles and macromolecules. However, the separation capacity is limited by the extreme conditions during ultracentrifugation, which can destroy cell membranes and other more labile structures. Additionally, these 'bulk' strategies are effective as long as the cell population to be separated is significantly different, with respect to size or density, from both the medium and the other cells in the population.

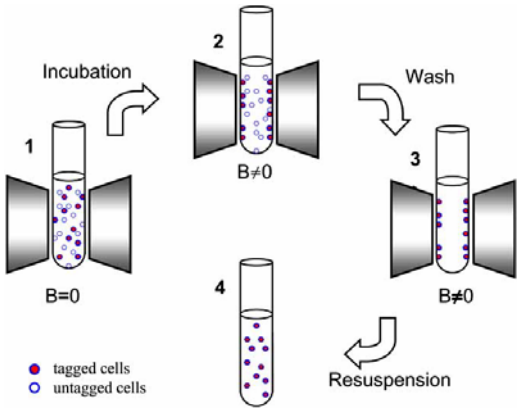

Fig. (5). A static magnetic separation method. By turning the field on, the cells attached to magnetic beads are fixed to the tube walls. Cells are resuspended by turning the field off alter removing untagged cells by washing.

Differently from the above methods, magnetic-based cell separation techniques do not rely on physical or chemical differences between the separated cells and the medium, but on the presence of a tagging element (i.e., the MNPs) that can be attached to the cell membrane with high specificity. Here, as for Drug Delivery, MRI or hyperthermia applications, the problems of functionalization and tagging are key issues that influence the final specificity of the whole process. The physical basis for magnetic cell separation methods is the force **F** generated on the attached MNPs when a magnetic particle with magnetic (dipole) moment **m** is placed in a *non-uniform* magnetic field **B**. It is important to notice that a *uniform* magnetic field $\mathbf{B_0}$ on a magnetic dipole does not exert net forces on it but only a torque that aligns it parallel to the field. However, when a non-uniform magnetic field **B** exists the force **F** exerted on a magnetic dipole with value **m** is related to the spatial variation of **B** through its spatial derivatives $\left(\partial\mathbf{B}/\partial x, \partial\mathbf{B}/\partial y, \partial\mathbf{B}/\partial z\right)$. For example, if a magnetic field changes from B = 0.1 to B = 1 T along

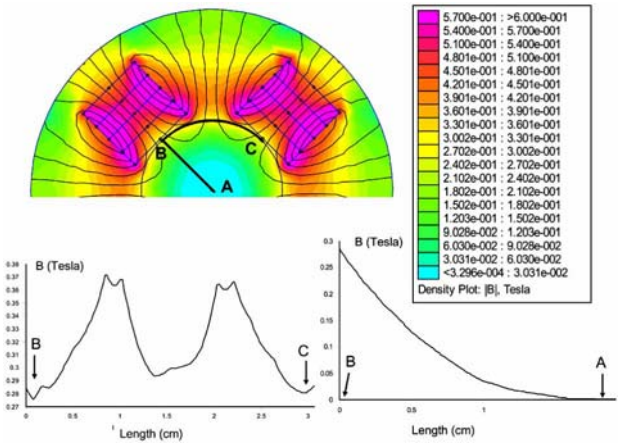

Fig. (6). Numerical simulation of magnetic field gradient for magnetic separation. Top view of a cylindrical device with four permanent $FeSm_5$ magnets placed at 90º each (only two are shown). The resulting induction fields B values are shown on the left scale. The solid lines indicate the direction along which the induction field profiles are calculated to maximize the radial forces. The profiles from B to C (circular) and from B to A (radial) are shown in the bottom graphs.

[1] Although it is called g-force and given in units of the gravitational g = 9.8 m/s2 constant, the actual effect is a strengthened acceleration during centrifugation, which is not originated in the Earth gravitational field. The performance of a centrifuge is given in RCF (relative centrifugal force) units, although the actual number that is computed is the centrifugal acceleration, in units of the Earth gravitational acceleration g = 9.8 m/s2. For example, a 1000 RCF value means that the objects will be accelerated 1000 times the g-value, or 9800 m/s.

any direction (e.g., the *x* axis) over a distance of $\Delta x = 0.1$ m, this variation of field amplitude will produce an *average* force $F_x = m \cdot \Delta B/\Delta x$ on a magnetic object in this region. For metallic iron, which has a magnetic moment $m = 222$ emu/g, (0.22 Am^2), the generated force will be $F_x = 0.22 \times (0.9 / 0.1) = 1.98$ Newtons, more than 200 times the gravitational force on the same piece of material.

In three dimensions, the variation of **B** has to be calculated along all *x, y* and *z* directions through the vector relationship $\mathbf{F} = (\mathbf{m}\cdot\nabla)\mathbf{B}$, which means that the net force **F** over a particle with moment **m** is nonzero only in the directions along which the magnetic field **B** is not homogeneous (i.e., has nonzero derivatives). This non-contact magnetic force is extensively used to separate living cells and smaller sub cellular units, making it a fundamental piece of biomedical research. The simplest way of having the required non-uniform field is by placing a number of magnetic poles (e.g., several pieces of permanent magnets) at one side of a test tube as schematized in Fig. (**5**). The magnetically tagged material will be trapped on the tube wall due to the magnetic force, so that the supernatant can be removed and the immobilized material washed and finally recovered by removing the tube (or turning off the field).

There are several magnet configurations capable of producing suitable magnetic field gradients for trapping purposes. One commercially used is the quadrupolar configuration that consists in four permanent magnets placed on the external side of a supporting tube, where the colloid is placed. This configuration produces four regions with maximum field along the circular perimeter of the tube, whereas B = 0 at the center of the tube. Fig. (**6**) shows the results of numerical simulations using four planar $FeSm_5$ magnets on a 4 cm diameter tube, and the variation of B along the tube wall and from the center.

Recently developed microfluidic platforms made possible the miniaturization of magnetic cell sorters, and current research indicates that integrated devices might be soon commercially available, within the lab-on-a-chip philosophy [79]. The concept of such a miniaturized device is that an heterogeneous cell population, targeted with MNPs of different sizes, can be injected into a microfluidic chamber where a magnetic field gradient perpendicular to the fluid velocity Fig. (**7**) generates a force capable to deflect each population proportionally to its magnetic moment. The inhomogeneous field is achieved by placing a permanent magnet on one side of the chamber so that an effective gradient is produced towards the magnetic pole. The deflection is proportional to the magnetophoretic mobility $\xi = \mathbf{v}/|\nabla \mathbf{B}^2|$, where **v** is the instantaneous velocity of the particle [80]. This parameter gives an estimation of how fast a given particle responds to a given magnetic force. The time to reach the collecting capillaries can be controlled by the input velocity, which in turn allows separation of different size windows.

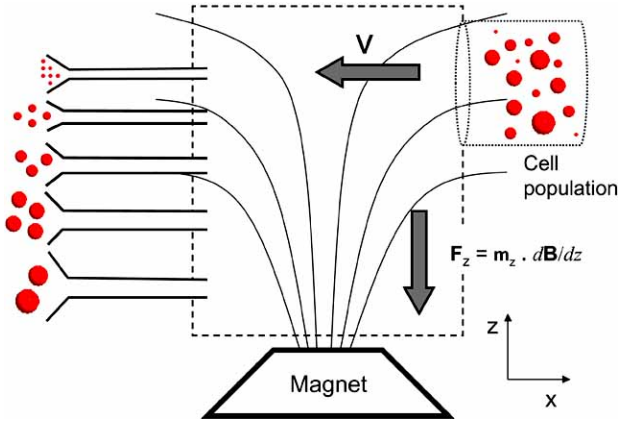

Fig. (7). Schematic view of a microfluidic cell sorter. A population containing different cell species, targeted with different particle sizes/amounts each, is injected with velocity **v** into the separation chamber. The magnetic field gradient deflects each size range by an amount $\Delta\mathbf{z}$ depending on the size of the cells and the applied flow rate.

Another 'flow-through' technique known as High Gradient Magnetic Separation [81] consists of a quadrupolar arrangement of magnets mounted concentrically on a tubular setup with thin annular geometry. This configuration is specifically designed to produce a radially symmetric magnetic field gradient in a plane perpendicular to the velocity field. As the cell mixture is carried along the channel by the input flow and passes through the magnetic field, the specific cell types tagged with immunospecific MNPs are driven toward the outer wall where some cell collector device retains the desired cells. This method provides two independent parameters **v** and **B** that can be tuned according to the magnetic responsiveness of the sorting material (i.e., the magnetophoretic mobility ξ) yielding large flow rates and wide sorting cell sizes.

These magnetic methods have reached high efficiency levels for cell separation, as compared with other driving forces such as electric and centrifugal, and also standard methods based on fluid-fluid interface separation [82-85]. All these techniques still face challenges regarding the purity of the final product since the starting liquid usually contains additional bioparticles, cell debris, non-tagged cells and other by-products, which can show similar behavior than the desired cells, depending on the driven force used. In spite of these difficulties, magnetic separation has been successfully tested for precise separation of specific cells in blood [86], gram-positive pathogens [87] and protein purification [88].

3.3. Magnetic Resonance Imaging (MRI)

Magnetic Resonance Imaging (MRI) is perhaps the most successful among the imaging techniques currently available. It is a non-invasive, non-destructive modality that can reconstruct both 2D and 3D images of an internal living structure, without limitation in volume or depth of the analyzed target. Since the 1980s, the implementation of dedicated hardware for MRI scanners has reduced the image acquisition time from the many-hour down to the second-scale [89], widening the applications to include fast dynamic processes. Additionally, signal processing and the development of high-sensitivity RF detectors have shifted the spatial resolution limit from the cm scale to about 10 μm, enabling *in vivo* imaging at microscopic resolution [90]. The above advantages have made MRI to become a most valuable technique for cancer diagnosis and therapy.

3.3.a. Physical Fundamentals

Any resonant technique is based on the existence of physical entities (e.g., electrons, nuclei, or molecules) that can be promoted from their ground state (taken as the zero-energy, E_0) to higher-energy excited states with E_1, E_2,…E_n. In the case of MRI, the resonant physical entities are the hydrogen nuclei (protons) that exist abundantly in living tissues. Protons placed in a homogeneous magnetic field B_0 can absorb electromagnetic (EM) waves carrying energies E_v satisfying $E_v = \Delta E$, where ΔE is the energy difference $\Delta E = E_1 - E_0$ between two nuclear levels [91]. Note that MRI involves a *magnetic* coupling between the magnetic-component of the EM waves and the *magnetic* moment of the resonant hydrogen nucleus (nuclear spin). Therefore the MRI is a *nuclear* resonance technique that gives information based on (but not restricted to) the *magnetic* properties of the biological samples. The signal from relaxation of the excited protons is captured through currents induced over a specific arrangement of pick-up coils, and finally the whole relaxation process is reconstructed computationally to obtain temporal or spatial (2D and 3D) images of the desired organ/tissues. The pick-up coils are needed to transmit and/or receive the MR signal, and for optimum signal-to-noise ratio the coils should cover only the working volume to be observed. Many types of pick-up coils have been designed for minimum noise (e.g., caging coils for

Table III. Clinically Approved Contrast Agents for MRI

Generic Name	Metal	Trade Name
Gadopentane dimeglumine	Gd	Magnevist ®
Gadoteridol	Gd	ProHance ®
Gadoterate	Gd	Dotarem ®
Gadodiaminde	Gd	Omniscan ®
Gadoversetamide	Gd	Optimark ®
Gadobutrol	Gd	Gadovist ®
Gadobenate dimeglumine	Gd	MultiHance®
Gadoxetic acid	Gd	Eovist ®
Magnafodipir trisodium	Mn	Teslacan ®
Ferumoxides	Fe_3O_4	Endorem®, Fedirex ®
Ferumoxil	Fe_3O_4	Lumirem ®, GastroMARK®
Ferucarbotran	Fe_3O_4	Resovist ®
Ferumoxtran	Fe_3O_4	Sinerem ® , Combidex ®

head and knee local studies), balancing observation volumes and sensitivity.

The energy $E_\nu = h\nu$ (where ν id the frequency and h is the Planck constant) of the EM waves used for resonant excitation will depend on the applied static field, B_0, through the relation

$$\upsilon = \frac{\gamma}{2\pi} B_0 \qquad \textbf{(XII)}$$

where the γ = 267.66 MHz/Tesla is Larmor frequency of the proton. Current commercial MRI platforms employ dc fields B_0 between 1 and 3 T, so that required RF frequencies are in the 50-100 MHz range. But companies have started to develop 7, 8 and 9 Tesla systems that imply the use of frequencies within the ~ 0.3 GHz range [92]. At these high RF frequencies dielectric coupling of the EMF with biological material cannot be neglected (see Fig. (**1**)), and indeed heating effects have been observed in phantoms using 8 Tesla MRI platforms [93]. The strategy used to visualize and track target cells by MRI is to tag them with a contrast agent, a ferrofluid containing biocompatible MNPs.

3.3.b. SPION-Based Contrast Agents

The purpose of injecting CA's is to *change* the relaxation rates (called T1 and T2) of the surrounding hydrogen atoms of the tagged cells, to the extent that a measurable change in signal intensity (contrast) is observed between particle-charged and normal tissues. The resulting differences in signals from various body tissues enable MRI to differentiate organs and to contrast benign and malignant (particle-loaded) tissues.

Gadolinium(III) was the first magnetic material clinically used as a contrast agent and still remains the foremost material in terms of total volume employed around the world [94]. This fact is probably related to the slow and costly process of preclinical validation of a new material intended for human uses, which delays the marketing of new products. However, different alternatives are being increasingly reported as good candidates for CAs, such as additional lanthanide ions and iron oxide nanoparticles [95]. Commercial contrast agents based on SPIONs are composed of a iron oxide core of 5 to 10 nm diameter (usually magnetite Fe_3O_4 or maghemite γ-Fe_2O_3), coated with a polysaccharide such as dextran for stabilization purposes, which results in a hydrodynamic size of ~150 nm diameter. These dextran-based coatings give them the generic names of ferumoxides (coated with low molecular weight dextran) and ferucarbotran (coated with carboxydextran) [95]. The products are recognized as safe and well tolerated, although the incidence of adverse reactions with iron oxides seems to be slightly higher than with gadolinium based agents. Although the Contrast Media Safety Committee of the European Society of Urogenital Radiology (ESUR) has proposed some working guidelines for magnetic resonance CAs, [96] general safety standards for the use of CAs based on comparative data from clinical trials with the available products are still lacking.

From the physical side, the performance of CAs regarding how it influences the relaxation of neighbor protons is proportional to the square of the saturation magnetic moment (M_S) of the particles, thus the design of new CAs requires optimized magnetic materials with large M_S values. All contrast agents based on MNPs make use of the large magnetic moment of iron-oxide subdomain particles, which can be 10^3 times larger than a single paramagnetic atom. The proximity of the magnetic particles to the desired target tissue is also a crucial parameter, since the magnitude of the interaction between a magnetic particle and neighboring protons is proportional to the sixth power of the inverse of the distance raised to (r^{-6}).

Although fundamentals of magnetic contrast agents regarding proton relaxation have been intensively investigated along the last years [8], imaging at the microscopic level imposes new challenges to the spatial resolution of RF signals coming from cells few micrometers apart. For example, passive (i.e., non-functionalized) particles usually accumulate around a target organ/tissue with a concentration distribution, but also partially around normal cells in the nearby. This generates a continuous gradient of magnetic field that avoids sharp definition of target's interface. The strategy for enhancing the sensitivity of MRI is therefore the development of high-specificity contrast agents that can be solely attached to the desired cells in tiny doses, avoiding the magnetic perturbation of healthy surrounding tissues.

An apparent consequence from the above discussion is that the efficiency of any MRI contrast agents as an early-diagnosis tool is intimately related to its capability of giving the strongest signal capable to be detected with the smallest amount of magnetic mate-

rial. Current CAs are composed of passive MNPs and thus there are far from the above specification. In general terms, the ideal efficiency would imply

a) Optimized magnetic properties of the magnetic-agent for *lowest* concentration per volume unit with the necessary sensitivity; and

b) Optimized particle functionalization for maximum selective affinity to targeted cells.

This many-folded optimization is not easy and has hampered the progress towards the synthesis of enhanced, 'smart' CAs, but it is accepted that going to the next step will require multidisciplinary expertise of many research groups from the different areas involved. In any case, there is some consensus about the fact that the key questions to be solved to make advanced CAs are related to:

§ selective binding to target cells to provide a local, specific enhancement

§ improved relaxational properties to decrease the detection threshold to low than 1mmol Fe/kg

§ prominent signal–to–noise enhancement to allow high resolution levels

§ long circulating half-life (hours) to expand the imaging time window

§ acceptable toxicity profile to be biologically safe

§ ease of production and clinical use to be economically and commercially sustainable

Applications of MRI with microscopic resolution levels have suggested the idea of MRI-based gene therapy [97], a modality aiming to record gene expression *in vivo*. The main challenge for such application is the development of magnetic nanoparticles designed at atomic scale, and functionalized with gene markers that will sense and track gene expression even before the clinical manifestation of the tracked disease. Even in the case of SPM nanoparticles, the above requirements imply a concept shift in synthesis and manipulation of NPs.

Most MRI contrast agents fall into two main categories: extracellular (unspecific) and cell-targeted (tissue-specific) agents, depending on the final biodistribution when inserted into the living organism. Regarding their physiological behavior, and the system target, they can be split in the following categories:

a) extracellular

b) hepatobiliary

c) reticuloendothelial system (RES) and

d) blood pool

On the other side, hybrid agents combining two of such functions have already been developed, for example gadobenate dimeglumine (Gd-BOPTA) and gadolinium-ethoxybenzyl-diethylenetriamine-pentaacetic acid (Gd-EOB-DTPA) CA's, which can be imaged in both the extracellular and hepatocyte phases [98]. In clinical MRI, the three different tissue-specific contrast agents are currently available namely SPIO, MnDPDP and Gd-BOPTA.

Tissue-specific CA's used in MRI of tumor (breast or liver) are designed to accumulate in normal tissue but not in focal lesions: while the signal from normal liver changes when these CAs are applied, they have nearly no effect on the signal acquired from e.g. metastatic liver deposits. Since the aim is to increase the signal difference, i.e. the contrast-to-noise ratios (CNR) of these lesions, any tissue-specific agent must have the potential to decrease the detection threshold.

The mechanism leading to an increase of CAs concentration in normal tissues but not to tumor lesions seems to be sub-cellular accumulation. In recent *in vitro* and *in vivo* experiments [99], iron-oxide (SPION) based nanoparticles functionalized with luteinizing hormone releasing hormone (LHRH) were used for detection of breast cancer cells. The experiments showed that LHRH-functionalized SPION accumulated in the cytosolic compartment of the target cells and formed clusters. On the other hand LHRH-SPIONs did not accumulate in livers of normal mice. *In vitro* results showed that LHRH-functionalized SPIONs were poorly incorporated by macrophages, whereas the amount of LHRH-SPION in the lungs was directly dependent on the number of metastatic cells. In contrast, unclothed SPIONs accumulated in the liver and showed poor affinity to the tumor, being undetectable in metastatic lung lesions.

Additional desired properties of tissue-specific CA's include long imaging window. Imaging may take place even several hours after the contrast agent injection. In this respect, SPION-based CA's are known to be more efficient than e.g. Gd-DTPA, i.e., lower doses are needed for obtaining comparable signals.

3.4. Hyperthermia

Within oncology therapeutics, hyperthermia is a general term for the rise of temperature above the physiologic level (in the 40°C -45°C range) within a targeted tumor without damaging the surrounding healthy tissue. The rationale of this therapy is based on solid evidence from preclinical data that the antitumor cytotoxicity of radiation can be enhanced by previous temperature increase of cells or tumor tissues. It is accepted that at the cellular level hyperthermia provokes morphological and physiological changes, such as the loss of integrins from the cell surface, which is thought to be a perturbing effect on metabolic pathways preceding cell death. The actual mechanisms active during hyperthermia treatments seem to be similar to those of radiation regarding cell cycle sensitivity and hypoxia [100]. The most extended method for reaching temperatures above the systemic values (i.e., 37·5°C) is based on the application of microwaves [101], although therapies involving laser [102] or ionizing radiation [103,104] have also been successfully applied to heat up malignant tissues. All these strategies are capable of easily rise the intracellular temperature to the degree needed for thermoablation, but also they all have undesired collateral effects such as ionization of genetic material (radiation) or lack of selectiveness (microwaves) that affect the surrounding healthy tissues [105, 106].

Nanostructures with tunable optical properties and biologically relevant size are one of the current strategies for selective thermal therapy. Recently, successful *in vitro* studies have been reported, based on functionalized gold nanorods that convert infrared (IR) radiation into heat that selectively destroys cancer cells [107]. The use of these nanostructures for hyperthermia is appealing, since temperature can be locally raised without affecting surrounding tissues. However, a drawback for IR radiation is the low penetration deep into tissues, which limits this technique to surface applications like melanoma cells.

The choice of the target temperature, as well as the physical source of heat generation, depends on factors such as tumor location, volume to be heated and microenvironmental factors (e.g. degree of vasculature or local pH). The synergistic interaction between heat and radiation therapy is recognized by the medical community, and has been already validated in preclinical studies [108]. However, there are no yet models that can describe the interplay between physical and biochemical cell mechanisms involved in thermosensitisation, heat-induced protein expression or cell apoptosis, on a microscopic basis. Recent efforts for elucidating these mechanisms have demonstrated that cell membrane and cytoskeleton are important loci of cell damage by both ionizing radiation and hyperthermia [109, 110].

Magnetic hyperthermia can be defined as the rise of temperature that can be accomplished remotely by means of external alternating magnetic field acting on MNPs at the targeted location.

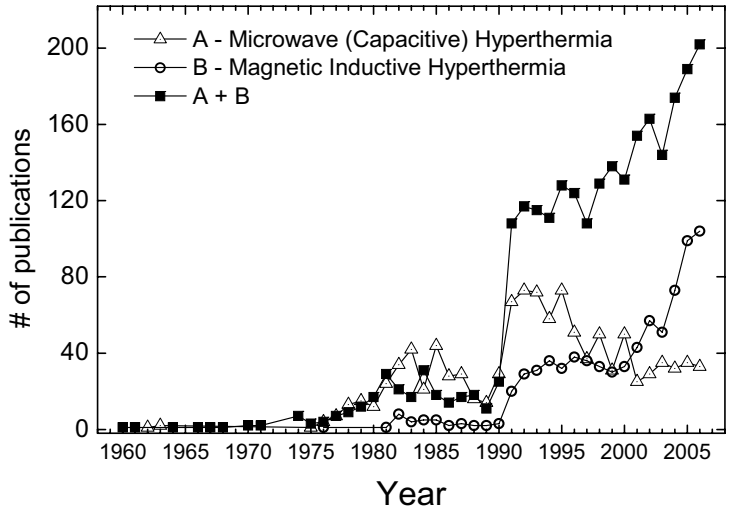

Fig. (8). Number of publications on hyperthermia since 1960. The evolution of published research of microwave (A) and magnetic (B) hyperthermia is shown. The establishment of MW hyperthermia is reflected as a sudden growth in reports during the 90's. A decade later, the development of novel magnetic nanoparticles yielded renewed interest in MFH.

There is a proliferation of names in the literature for identifying this new technique, e.g., ferromagnetic hyperthermia, magnetic fluid hyperthermia, magneto-thermo-cytolysis, magnetic-inducted hyperthermia, magneto-thermoablation, alternating magnetic field (AMF) or intracellular hyperthermia. Given this lack of consensus we shall use hereafter the term Magnetic Fluid Hyperthermia (MFH) because it embraces the three basic characteristics involved.

It is important to note that the EM radiation used by MFH belongs to a frequency region where the heating effects on living tissues are negligible. Therefore, differently from other hyperthermia methods, MFH needs a heating agent (i.e., the magnetic nanoparticles) placed at the targeted cells in order to produce the temperature increase. This difference if the main reason of the potential advantages of MFH over alternative strategies, since MNPs can be in principle attached exclusively to (or even introduced into) tumoral cells to heat them with minimum influence on the surrounding healthy tissues. Therefore the success of this approach depends critically of the ability to attach a given particle on those cells that are to be killed (i.e., the 'targeting problem'). As discussed in see Sec. 3.1 this is a many-folded biochemical, biological and medical issue, and continuous improvements are being reported periodically in the literature. Indeed, the advancement in 'cell targeting' have boosted a renewed interest in MFH in the last few years (see Fig. (**8**), because a molecular-level targeting of cells with MNPs is the prerequisite for efficient heating of the targeted tissue. This may, in turn, allow overcoming the lack of rigorous thermal dosimetric data necessary to obtain verifiable prescriptions for MFH clinical uses as a stand-alone therapy.

The underlying physical mechanisms of MFH are related to the energy dissipation when a ferromagnetic material is placed on an external alternating magnetic field. The basic concepts were already discussed in section. 2.4. In physiological conditions there are different effects to be considered for power losses: a) magnetic losses through domain wall displacements (in multi-domain particles, see section 2.3), Néel relaxation (in single domain particles); and b) energy loss from mechanical rotation of the particles, acting against viscous forces of the liquid medium (Brownian losses). The dominant process will depend on the specific particles used and the applied frequency range. From the point of view of the biological applications, the microscopic mechanisms that produce the cellular hyperthermia are still being discussed, even to the point of casting doubts on the existence of intracellular hyperthermia [111]. As already mentioned, the technique is based on the power losses of MNPS injected in the tumoral region by the application of a variable external magnetic field. However, and in spite of empirical work on therapeutic effects (both *in vitro* and *in vivo*) reported in the literature [112], the lack of knowledge on the fundamental mechanisms involved has prevented the implementation of clinical protocols of routine use. In any case, to identify the mechanisms of magnetic losses of a nanostructured material in physiological condi-

Table IV . Values of SAR as Reported for Several Magnetic Colloids Having Different Particle Properties. Note the Different Conditions (B, *f*) Under Which the Experiments are Carried Out, Hampering a Comparative Analysis of the Data

Material	Core Radius (nm)	Hydr Radius (nm)	Liquid	SAR	Units	*f* (kHz)	B (kA/m)	Conc.	Ref
γ-Fe_2O_3	5	7	aqueous	13.8	kW/mol Fe	500	12.5	10 mmol/m^3	[113]
Fe_3O_4	8	10	aqueous	84	W/g	400	6.5	1 g/ml	[114]
Fe_3O_4	3-10	200	aqueous	56	W/g	400	6.5	1 g/ml	[114]
Fe_3O_4	3-10	280	aqueous	31	W/g	400	6.5	1 g/ml	[114]
γ-Fe_2O_3	< 1000	>2000	tissue	80	mW/g	53	40	0.84 mg/g tissue	[115]
γ-Fe_2O_3	< 1000	>2000	tissue	173	mW/g	53	40	1.8 mg/g tissue	[115]
Fe_3O_4	13	N/A	aqueous	39.4	W/g of Fe	80	32.5	2 g/l	[116]
Fe_3O_4	81	N/A	aqueous	63.7	W/g of Fe	80	32.5	2 g/l	[116]
Fe_3O_4	416	N/A	aqueous	28.9	W/g of Fe	80	32.5	2 g/l	[116]

tions is an unavoidable step towards the design of therapeutic materials for biomedicine.

The heating power of magnetic nanoparticles given by the SAR in W/kg, is obtained from the experimental heating curves versus time, based on the initial ΔT temperature rising interval through the definition

$$SAR = \frac{C_S}{m_{Fe}}\left(m_{FF}\frac{\Delta T}{\Delta t}\right) \quad \textbf{(XIII)}$$

where C_S is the heat capacity (in J K^{-1}) of the colloid and m_{Fe} and m_{FF} are the masses of magnetic material and colloid, respectively. The experimental SAR values previously reported for different magnetic colloids (Table **IV**) show strong sample-dependency. The large variability of values even for 'similar' colloids also suggests that more than a single absorption mechanism may be involved, yielding a multiplicity of parameters that govern the overall process. Moreover, the functional dependence of SAR values on these experimental parameters (e.g., applied field, frequency or particle concentration) is unknown, thus comparison by extrapolation between different experimental setups is not reliable.

For *in vivo* applications, the measure of SAR is further obscured by the fact that the final particle concentration at the targeted (heated) sites is usually unknown. Jordan *et al.* [113] have shown that SAR can be optimized through magnetic fractionation of the starting colloid, i.e., by selecting a small particle size window from the original size distribution. In addition to particle size and shape influence on heating power [114-116], the magnetic field amplitude and frequency must be considered when comparing experiments in Table **IV**.

3.4.a. Instrumentation

In spite the growing amount of basic research on MFH both *in vitro* and *in vivo*, there are three main obstacles that have withhold until now the development of daily clinical protocols: 1) the difficulty of controlling the biochemical mechanisms for specific targeting the MNPs onto neoplasic cells; 2) the lack of complete knowledge of the basic mechanisms involved in magnetic losses of nanostructured materials in physiological conditions; and 3) the technical difficulties to develop magnetic field applicators at the frequencies and field values, with a concurrent compliance of the safety regulations demanded in clinical use. This section will refer to the latter problem, giving a brief description of some strategies and accomplishments along the last years.

Magnetic field applicators for SAR measurements in biological samples are designed to work between 100 and 800 kHz. This frequency range is the same used for AM broadcast in most western countries, and more specifically it corresponds to the low frequency part of the AM bands called long-wave (LW) and medium-wave (MW) bands. Lower frequencies (<100 kHz) are usually avoided for efficiency reasons, since most mechanisms for magnetic losses are proportional to f^n with n > 1 (see 2.4). On the other side, the high-frequency limits attainable are imposed by the electrical coupling of the EM waves with biological matter that provokes dielectric heating, a well-known effect for the microwave range. Government regulations in the United States and European countries establish safe levels for human exposure to RF energy. For example, several European countries are basing guidelines on exposure criteria developed by the International Committee on Nonionizing Radiation Protection (ICNIRP) [117]. In 1998 the ICNIRP established a SAR threshold of 4 W/kg (for adverse effects) in the low-RF range (ca. 1 kHz). These exposure limits are expressed in terms of electric and magnetic field strength and power density for transmitters operating at frequencies from 300 kHz to 100 GHz are shown in Table **V**. The FCC in the United States also adopted limits for localized ("partial body") absorption in terms of SAR that apply to certain portable transmitting devices such as hand-held cellular telephones.

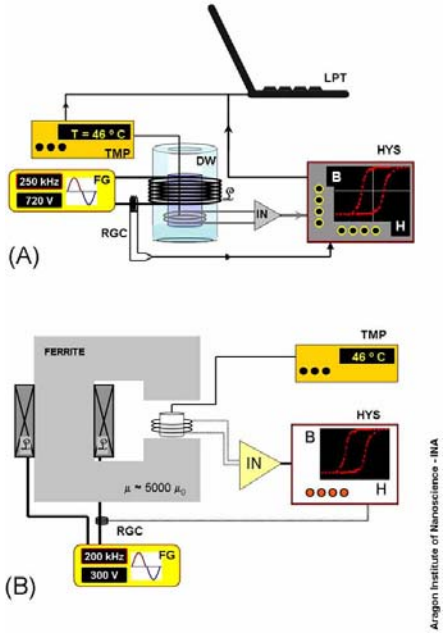

Fig. (9). Two common configurations for laboratory MFH applications. (A) The Dewar (DW) containing the samples is places inside the coil (L). A current/voltage source (FG) gives the electrical current needed to create a magnetic field inside the coil. See text for details. The gapped-ferrite setup (B) is similar to (A) but the magnetic flux is concentrated using a high permeability, high frequency ferrite.

Inductive heating includes three complementary mechanisms: EM induction, skin effect, and heat transfer. These mechanisms are described similarly than those of a transformer, although the purpose here is to maximize the power loses at the sample (i.e., the 'secondary' coil in a transformer). Different topologies can be constructed to efficiently deliver the required amount of power to the

Table V. Maximum Permissible Exposure Values of EMF Parameters: Magnetic Field H, Power Density S and Specific Absorption Rate SAR, at Low RF Frequencies *f*, as Determined by the *Federal Communications Commission (FCC).* (See Ref. [41])

Exposure	Frequency *f*	H (A/m)	S (mW/cm^2)	Partial-body SAR ♣	Whole-body SAR ♣
Controlled §	300 kHz to 3 MHz	1.63	100	< 8 W/kg	< 400 mW/kg
Uncontrolled§§	300 kHz to 1340 kHz	1.63	100	< 1.6 W/kg	< 80 mW/kg

§ Controlled limits apply to persons exposed as a consequence of their employment provided those persons are fully aware of the potential for, and can exercise control over, the exposure.
§§ Uncontrolled exposures apply in situations in which the general public may be exposed, that are not fully aware of the potential for, or cannot exercise control over, the exposure.
♣ Valid for 100 kHz to 6 GHz range.

samples, and this power depends critically of the working volume where the field is required for applications. Two of the most usual types are the half-bridge series resonant converter and the quasi-resonant converter, each one having its pros and cons. A half-bridge resonant converter is more stable for switching and easy to adapt to hyperthermia experiments because some tolerance in the final frequency value is possible. On the other hand, this architecture needs two switching circuits working synchronized at half-cycles, thus each working cycle is electrically more complex.

The two basic configurations shown in Fig. (**9**) are designed as a resonant LC tank, with capacity C and inductance L adjusted for resonating at the desired frequency. In this way, the real power provided by the source is much less than the reactive power circulating inside the LC tank. The power source used for the experimental setup of Fig. (**9**) is a switching source of variable voltage and frequency, based on a two-MosFET half-bridge with a bootstrap circuit. The bridge provides a square voltage wave that is smoothed by the LC series circuit. With the help of an ADC converter (IN) and a Rogowsky coil (RGC) both the induction B and the applied field H can be traced in an oscilloscope (HYS). These data, together with the temperature increase vs. time (measured with a fiber optic thermometer, TMP) is stored and handled in a computer (LPT).

The two configurations shown in Fig. (**9**) can deliver power required for attaining ac magnetic fields of amplitude 100-500 Oe within the LW radio band range, with 1% homogeneous field within a working space of 100-1000 cm^3. Both the single air-core solenoid and the ferrite-gap configurations of can be used, and the choice of the final geometry will depend on the type of sample to be measured, as well as the type of complementary equipment for measuring temperature and magnetic properties of the sample.

From the electrical point of view, the gapped configuration has the advantage of being 'inductance-tunable': by changing the size of the air gap the total value of the induction L of the solenoid + ferrite core can be adjusted to match a given frequency of the power source.

3.4.b. In-vitro Applications

For clinical applications, the granular materials should present low levels of toxicity, as well as a high saturation magnetic moment in order to minimize the doses required for temperature increase. As mentioned in sec. 2.2 magnetite (Fe_3O_4) has shown the lowest toxicity index in pre-clinic tests and therefore their use in MRI protocols is preferred when negative contrast is required. From the metabolic point of view, increased temperatures usually alter gene expression, resulting in over-expression of a family of heat-shock proteins (HSP) [118]. This result have been considered by Ito *et al.* [119] to propose a combination therapy using immunotherapy and hyperthermia. These authors reported for the first time that the combination of hyperthermia and local injection of GM-CSF (a cytokine related to the maturation of antigen-present cells) resulted in antitumor response against malignant melanoma.

As the agent coupling the system with the external magnetic field is the magnetic moment of the particles, the magnetic properties of the grains are a relevant parameter for controlling any desired response of the whole system regarding dissipated power. Particle size and shape determine the anisotropy energy barrier of that particle, and therefore is an essential parameter for the reversion of magnetic moments in an ac field. Due to the lack of comprehensive models for these phenomena *in vitro* or *in vivo*, it is quite important the design of systematic experiments to measure the kinematics and dynamics of the power dissipation during an ac cycle. This seems to be the prerequisite for the synthesis of more efficient power-absorbing magnetic ferrofluids.

3.4.c. In-vivo Applications

Early experimental evidence about the viability of inducing intra-cellular hyperthermia by ac magnetic fields was published by Gordon *et al.* [120], who applied magnetite nanoparticles to mammary carcinoma in rat model. *Ex vivo* studies performed by Yanase *et al.* using magnetically loaded cationic liposomes (MCL) have showed the viability of reaching over 43°C in solid subcutaneous rat tumors [121] after repeatedly applying alternate fields during 30 min intervals. The total amount of Fe_3O_4 injected was 3 mg, and the frequency used in these experiments was 118 kHz. No information about field amplitude was given. The same group has reported *in vivo* studies with magnetite-loaded MCL on F344 rats, where complete tumor regression after 30 days was reported, without tumor regrowth for a 3 month period [122]. Similarly, Ito *et al.* have also reported complete regression of mouse mammary carcinoma, of 15 mm size, by multi-application protocols [112]. Control of tumor growth for periods of 20 days was achieved by using imnuno-targeted MCLs [123], with repeated applications. Although the efficiency of MCLs in hyperthermia applications is appealing, there is still the need of determining the bio-distribution and elimination pathways after injection.

In 1997 Jordan *et al.* reported the successful use of magnetite nanoparticles of ca. 3 nm in mammary carcinoma of mice [124]. After local injection the magnetic trapping technique was used to retain and increase locally the concentration of particles. The experiments were conducted at 12.5 kA m^{-1} maximum field at 520 kHz, with a particle concentration of 17 mg/ g tissue. This group reported inhomogeneous necrosis of tumor tissue, attributing this effect to inhomogeneities of the magnetic particles.

A recent study about magnetite-based colloids injected into human breast adenocarcinoma implanted into mice also showed necrosis of tumor tissue after repeated field applications. However in this study the local temperature raised to 73 C in some points, a process termed magnetic thermal ablation [125].

Up to now, the only MFH-based clinical trial has been conducted at the University Medicine Berlin by Jordan's group. The whole system has been commercially developed by MagForce Nanotechnologies AC, [126] and consists of two complementary technologies: a) the magnetic field applicator (MFH®300F) working at 100 kHz, with fields from 0 to 18 kAm/m that meets safety standards for clinical trials, and b) the organically-coated iron-based colloids of 15 nm size (MagForce®). The system is used in conjunction with MR and CT-generated 3D images of the targeted areas, and computer simulations of the heat distribution based on the observed distribution of MNPs. This complete setup has already demonstrated the feasibility of MNPs as cancer therapy agents in recurrent prostate carcinoma [126], and will probably increase its efficiency once tumor-targeted MNPs of high specificity are available.

4. CONCLUSIONS AND PERSPECTIVES

The first steps have been successfully achieved towards new synthesis routes for magnetic colloids with precise control of particle size and distribution. These NPs have been the 'generation zero' of the next multi-function systems with specific surface properties for detecting, targeting and signaling any desired biological target. The advancements on surface biochemistry will surely play a key role for these 'smart' biomedical tools. Concurrently, the understanding of intrinsic and collective magnetic properties of nanoparticles has been pushed to new frontiers by unexpected phenomena at nanometric scales. With this development of controlled magnetic agent, the foreseen future of clinical applications such as MRI, PET, or MFH is to act at nanometer levels with molecular detection resolution. For this goal to be achieved, concurrent improvements in signal detection and processing are also needed.

Although we have witnessed big progress along the last decade, future success in the biomedical area of nanoparticle applications will depend on the level of integration between the several fields involved. In particular, a deeper understanding of the molecular mechanisms underlying early stages of cancer is a requisite if new oncologic NPs-based therapies are to be designed.

ACKNOWLEDGEMENTS

This work has been supported by the Spanish Projects Nanoscience Action NAN200409270-C3-1/2 and Consolider Ingenio CSD2006-00012. GFG acknowledges support from the Spanish MEC through the Ramon y Cajal program.

REFERENCES

[1] Barrat, G. *Cell. Mol. Life Sci.*, **2003**, *60*, 21.
[2] Wellinghausen, N.; Wirths, B.; Essig, A.; Wassill, L. *J. Clin. Microbiol.*, **2004**, *42*, 3147.
[3] Bradwell, A.R.; Carr-Smith, H.D.; Mead, G.P.; Tang, L.X.; Showell, P.J.; Drayson, M.T.; Drew, R. *Clin. Chem.*, **2001**, *47*, 2069.
[4] Ortega-Vinuesa, J.L.; Hidalgo-Álvarez, R.; de las Nieves, F.J.; Davey, C.L.; Newman, D.J.; Price, C.P. *J. Colloid Interface Sci.*, **1998**, *204*, 300.
[5] Katz, L.C.; Burkhalter, A.; Dreyer, W.J. *Nature*, **1984**, *310*, 498.
[6] Donaldson, I.M.L. *J. R. Soc. Med.*, **2005**, *98*, 572.
[7] Pankhurst, Q.A.; Connolly, J.; Jones, S.K.; Dobson, J. *J. Phys. D: Appl. Phys.*, **2003**, *36*, R167.
[8] Hafeli, U.; Schutt, W.; Teller, J.; Zborowski, M. (Eds), *"Scientific and Clinical Applications of Magnetic Carriers"*, Plenum Press, New York, **1997**.
[9] Klostranec, J.M.; Chan, W.C.W. *Adv. Mater.,* **2006**, *18*, 1953.
[10] Tartaj, P.; Morales, M.D.; Veintemillas-Verdaguer, S.; Gonzalez-Carreño, T.; Serna, C.J. *J. Phys. D-Appl. Phys.*, **2003**, *36*, R182.
[11] Charles, P.; Elliot, P. *"Handbook of Biological Effects of electromagnetic Fields"* CRC Press Pub., **1995**.
[12] Hayes, B. *Am. Sci.*, **2002**, *90*, 212.
[13] Riabinina, D.; Durand, C.; Chaker, M.; Rowell, N.; Rosei, F. *Nanotechnology*, **2006**, *17*, 2152.
[14] Goya, G.F. *Solid State Commun*., **2004**, *130*, 783.
[15] Ishikawa, Y.; Shibata, N.; Fukatsu, S. *J. Cryst. Growth*, **1997**, *175*, 493.
[16] Ferlauto, A.S.; Alvarez, F.; Fonseca, F.C.; Goya, G.F.; Jardim, R.F. *J. Metastable Nanocryst. Mater.*, **2004**, *20-21*, 700.
[17] Fernandez-Pacheco, R.; Arruebo, M.; Marquina, C.; Ibarra, R.; Arbiol, J.; Santamaria, J. *Nanotechnology*, **2006**, *17*, 1188.
[18] Bomati-Miguel, O.; Leconte, Y.; Morales, M.P.; Herlin-Boime, N.; Veintemillas-Verdaguer, S. *J. Magn. Magn. Mater.*, **2005**, *290*, 272.
[19] Wu, K.T.; Kuo, P.C.; Yao, Y.D.; Tsai, E.H. *IEEE Trans. Magn.,* **2001**, *37*, 2651.
[20] Endo, M.; Kim, Y.A.; Ezaka, M.; Osada, K.; Yanagisawa, T.; Hayashi, T.; Terrones, M.; Dresselhaus, M.S. *Nanoletters,* **2003**, *3* , 723.
[21] Mathur, S.; Veith, M.; Rapalaviciute, R.; Shen, H.; Goya, G.F.; Martins, W.L.; Berquo, T.S. *Chem. Mater.*, **2004**, *16*, 1906.
[22] For a comprehensive review on magnetic fluid applications see: Odenbach S. *J. Phys.: Condens. Matter.,* **2004**, *16*, R1135.
[23] Rosensweig, R.E.; *"Ferrohydrodynamics"*, Cambridge University Press, Cambridge, **1985**.
[24] Marchal, G.; Vanhecke, P.; Demaerel, P.; Decrop, E.; Kennis, C.; Baert, A..L.; Vanderschueren, E. *Am. J. Roentgenol*., **1989**, *152*, 771.
[25] Cullity, B.D. *"Introduction to Magnetic Materials"*, (Addison Wesley, Reading MA 1972).
[26] Frenkel, J.; Dorfman, J. *Nature*, **1930**, *126*, 274.
[27] Kittel, C. *Phys. Rev*., **1946**, *70*, 965.
[28] Néel, M. L. *Ann. Geophys*., 1949, **5**, 99.
[29] Eberl, D.D.; Kile, D.E.; Drits, V.A. *Am. Mineral.*, **2002**, *87*, 1235.
[30] Fonseca, F.C.; Ferlauto, A.S.; Alvarez, F.; Goya, G.F.; Jardim, R.F. *J. Appl. Phys.,* **2005**, *97*, 044313.
[31] Lima, Jr. E.; Brandl, A. L.; Arelaro, A. D.; Goya, G.F. *J. Appl. Phys.,* **2006**, *99*, 083908.
[32] De Wulf, M.; Makaveev, D.; Dupre, L.; Permiakov, V.; Melkebeek, J. *J. Appl. Phys*., **2003**, *93*, 8543.
[33] Grossinger, R.; Sato, R.; Holzer, D.; Dahlgren, M. *Adv. Eng. Mater.,* **2003**, *5*, 285.
[34] Kaminski, W. *AMSE J. Heat Transfer*, **1990**, *112*, 555.
[35] Mitra, K.; Kumar, S.; Vedavarz, A.; Moallemi, M. K. *AMSE J. Heat Transfer*, **1995**, *117*, 568.
[36] Saidane, A.; Aliouat, S.; Benzohra, M.; Ketata, M. *J. Food Eng.*, **2005***, 68*, 491.
[37] Pennes, H.H. *J. Appl. Physiol.*, **1948**, *2*, 93.
[38] Brix, G.; Seebass, M.; Hellwig, G.; Griebel, J. *Magn. Res. Imaging*, **2002**, *20*, 65.
[39] Liu, X.; Li, J.; Gong, X.; Zhang, D. *Ultrasonics*, article in press (doi:10.1016/j.ultras.2006.06.035)
[40] Andra, W.; d'Ambly, C.G.; Hergt, R.; Hilger, I.; Kaiser, W.A. *J. Magn. Magn. Mater.*, **1999**, *194*, 197.
[41] Federal Communications Commission (FCC), "*Questions and Answers About the Biological Effects and Potential Hazards of Radiofrequency Electromagnetic Fields."*, OET Bulletin No. 56, 1999. (http://www.fcc.gov/oet/rfsafety/background.html)
[42] Neuberger, T.; Schöpf, B.; Hofmann, H.; Hofmann, M.; von Rechenberg, B. *J. Magn. Magn. Mater.*, **2005**, *293*, 483.
[43] Susuki, M.; Shinkai, M.; Yanase, M.; Ito, A.; Honda, H.; Koboyash, T. *Jpn. J. Hyperthermic Oncol.,* **1999**, *15*, 79.
[44] Asmatulu, R.; Zalich, M. A.; Claus, R.O.; Riffle, J.S. *J. Magn. Magn. Mater.,* **2005**, *292*, 108.
[45] Moharraj, V. J.; Chen, Y. *Trop. J. Pharm. Res.*, **2006**, *5*, 461.
[46] Maeda, H.; Wu, J.; Sawa, T.; Matsumura, Y.; Hori, K.J. *J. Control. Release,* **2000**, *65*, 271.
[47] Brannon-Peppas, L.; Blanchette, J.O. *Adv. Drug Deliv. Syst.,* **2004**, *56*, 1649.
[48] Duguet, E.; Vasseur, S.; Mornet, S.; Devoisselle, J.-M. *Nanomedicine,* **2006**, *1*, 157.
[49] Sinha, R.; Kim, G.J.; Nie, S.; Shin, D.M. *Mol. Cancer Ther.,* **2006**, *5*, 1909.
[50] Cancer NANOTECHNOLOGY PLAN (2004). A strategic initiative to transform clinical oncology and basis research through the directed application of nanotechnology BCI, NIH, USA. (www.nano.cancer.gov/ alliance_cancer_nanotechnology_plan.pdf).
[51] Sledge, G.; Miller, K. *Eur. J. Cancer,* **2003**, *39,* 1668.
[52] Lu, Y.J.; Low, P.S. *Adv. Drug Deliv. Rev.,* 2002, *54*(5), 675.
[53] Hilgenbrink, A.R.; Low, P.S. *J. Pharm. Sci.*, **2005**, *94*, 2135.
[54] Sudimack, J.; Lee, R.J. *Adv. Drug Deliv. Rev.*, **2000**, *41*, 147.
[55] Choi, H.; Choi, S.R.; Zhou, R.; Kung, H.F.; Chen, I.W. *Acad. Rad.*, **2004**, *11*, 996.
[56] Sun, C.; Sze, R.; Zhang, M.Q. *J. Biomed. Mater. Res. A*, **2006**, *78A*, 550.
[57] Ambrosini, G.; Adida, C.; Altieri, D.C. *Nat. Med.*, **1997**, 3*,* 917.
[58] Altieri, D.C. *Prog. Cell Cycle Res*., **2003**, *5*, 447.
[59] Reed, J.C.; Wilson, D.B. *Clin. Cancer Res.*, **2003**, *9*, 6319.
[60] Fayette, J.; Soria, J.C.; Armand, J.P. *Pathol. Biol.,* **2006**, *54*, 199.
[61] Shao, Z.M.; Nguyen, M. *Front. Biosci.*, **2002**, *7*, 33.
[62] Lim, S.T.; Levine, A.M. *Hematology*, **2005**, *10*, 11.
[63] Wu, Y.; Zhong, Z.J.; Huber, J.; Bassi, R.; Finnerty, B.; Corcoran, E.; Li, H.L.; Navarro, E.; Balderes, P.; Jimenez, X.; Koo, H.; Mangalampalli, V.R.M.; Ludwig, D.L.; Tonra, J.R.; Hicklin, D.J. *Clin. Cancer Res.*, **2006**, *12*, 6573.
[64] Cardones, A.R.; Banez, L.L. *Curr. Pharm. Des*., **2006**, *12*, 387.
[65] Jain, K. K. *Trends Biotechnol*., **2006**, *24*, 143.
[66] Gupta, A.K.; Gupta, M. *Biomaterials*, **2005**, *26,* 3995.
[67] Smith, J.E.; Wang, L.; Tan, W. *Trends in Analytical Chem.,* **2006**, *25*, 848.
[68] Turková J. *J. Chromatogr. B,* **1999**, *722*, 11.
[69] Fuentes, M.; Mateo, C.; Guisán, J.M.; Fernández-Lafuente, R. *Biosens. Biolectron.*, **2005**, *20*, 1380.
[70] Brigger, I.; Dubernet, C.; Couvreur, P. *Adv. Drug Deliv. Rev.*, **2002**, *54*, 631.
[71] Moroz, P.; Metcalf, C.; Gray, B.N. *BioMetals*, **2003**, *16*, 455.
[72] Storm, G.; Belliot, S.O.; Daemen, T.; Lasic, D. *Adv. Drug Deliv. Rev.*, **1995**, *17*, 31.
[73] Choi, S. W.; Kim, W. S.; Kim, J.H. *J. Dispersion Sci. Technol.,* **2003**, *24*, 475.
[74] Michel, R.; Pasche, S.; Textor, M.; Castner, D.G. *Langmuir,* **2005**, *21*, 12327.
[75] Moore, A.; Marecos, E.; Bogdanov, A.; Weissleder, R. *Radiology,* **2000**, *214*, 568.
[76] Kaul, G.; Amiji, M. *J. Drug. Target*, **2004**, *12*, 585.
[78] Micke, P.; Ostman, A. *Lung Cancer,* **2004**, *45*, 163.
[77] Allen, T.M. *Trends Pharmacol. Sci.,* **1994**, *15*, 215.
[79] Ramadan, Q.; Samper, V.; Poenar, D.; Yu, C. *Biomed. Microdevices,* **2006**, *8*, 151.
[80] Häfeli, U.O.; Lobedann, M.A.; Steingroewer, J.; Moore L. R.; Riffle, J. *J. Magn. Magn. Mater.*, **2005**, *293*, 224.
[81] Thomas, T. E.; Abraham, S. J.; Otter, A. J.; Blackmore, E. W.; Lansdorp, P. M. *J. Immunol. Methods*, **1992**, *154*, 245.
[82] Ambler, C.M. *Ind. Eng. Chem.*, **1961**, *53*, 430.
[83] Tan, K.H. *J. Biol. Chem.,* **1972**, *247*, 3278.
[84] Bahr, K.H. *Chem. Eng. Sci.,* **1992**, *47*, 11.
[85] Comella, K. *Cytometry*, **2001**, *45*, 285.
[86] Toner, M.; Irimia, D. *Ann. Rev. Biomed. Eng.*, **2005**, *7*, 77.
[87] Lin, Y.S.; Tsai, P.J.; Weng, M.F.; Chen, Y.C. *Anal. Chem.,* **2005**, *77*, 1753.
[88] Franzreb, M.; Siemann-Herzberg, M.; Hobley, T.J.; Thomas, O.R.T. *Appl. Microbiol. Biotechnol.*, **2006**, *70*, 505.
[89] Zhang, X.; Webb, A. *Concept. Magn. Reson. B,* **2005**, *24B*, 6.
[90] Johnson, G.A.; Benveniste, H.; Black, R.D.; Hedlund L.W.; Maronpot R.R. and Smith B.R., *Mag. Reson.,* **1993**, *Q9*, 1.
[91] Liney, G. "*MRI from A to Z : a definitive guide for medical professionals",* Cambridge University Press, **2005**.
[92] Vaughan, J. T.; DelaBarre, L.; Snyder, C.; Adriany, G.; Collins, C.M.; Van De Moortele, P.-F.; Moeller, S.; Ritter, J.; Strupp, J.; Andersen, P.; Tian, J.; Smith, M.B.; Ugurbil, K. *Proceedings of The International Society of Magnetic Resonance in Medicine Annual Meeting*, Miami, Florida, **2005**, *953*.
[93] Kangarlu, A.; Shellock, F.G.; Chakeres, D.W. *J. Magn. Res. Imaging,* **2003**, *17*, 220.
[94] Bottrill, M.; Nicholas, L.K.; Long, N.J.*Chem. Soc. Rev.*, **2006**, *35*, 557.
[95] Reimer, P.; Balzer, T. *Eur. Radiol.*, **2003**, *13*, 1266.

[96] Thomsen.; H.S.; Morcos, S.K. *J. Abdom. Imag.*, **2006**, *31*, 131.
[97] Bremer, C.; Weissleder, R. *Acad. Radiol.,* **2001**, *8*, 15.
[98] Hyslop, W. B.; Semelka, R.C. *Top. Mag. Reson. Imaging,* **2005**, *16*, 3.
[99] Leuschner, C.; Kumar, S.S.R.C.; Hansel, W.; Soboyejo, W.; Zhou, J.; Hormes, J. *Breast Cancer Res. Tr.*, **2006**, *99*, 163.
[100] Kampinga, H.H.; Dikomey, E. *Int. J. Radiat. Biol.,* **2001**, *77*, 399. *See also the work of* Halicka, H.D.; Seiter, K.; Feldman, E.J.; Traganos, F.; Mittelman, A.; Ahmed, T.; Darzynkiewicz, Z. *Apoptosis*, **199**7, *2*, 25.
[101] Gardner, R.A.; Vargas, H.I.; Block, J.B.; Vogel, C.L.; Fenn, A.J.; Kuehl, G.V.; Doval, M. *Ann. Surg. Oncol.*, **2002**, *9*, 326.
[102] Shields, C.L.; Shields, J.A. *Curr. Opin. Ophthalmol.*, **2004**, *15*, 244.
[103] Kampinga, H.H. *Int. J. Hyperthermia,* **2006**, *22*, 191.
[104] Gottlieb, C.F.; Seibert, G.B.; Block, N.L. *Radiology*, **1988**, *169*, 243.
[105] Cockroft, D.L.; New, D.A.T. *Nature,* **1975**, *258*, 604.
[106] He, X.; McGee, S.; Coad, J.E.; Schmidlin, F.; Iaizzo, P.A.; Swanlund, D.J.; Kluge, S.; Rudie, E.; Bischof, J.C. *Int. J. Hyperthermia,* **2004**, *20*, 567.
[107] Huang, X.; El-Sayed, I.H.; Qian, W.; El-Sayed, M.A. *J. Amer. Chem. Soc.*, **2006**, 128, 2115.
[108] Jones, E.L.; Oleson, J.R.; Prosnitz, L.R.; Jones, E.L.; Samulski, T.V.; Vujaskovic, Z.; Yu, D.; Sanders, L.L.; Dewhirst, M.W. *J. Clin. Oncol.,* **2005**, *23*, 3079.
[109] Coakley, W.T. *Symp. Soc. Exp. Biol.,* **1987**, *41*, 187.
[110] Lepock, J.R. *Int. J. Hyperthermia,* **2003**, *19*, 252.
[111] Rabin, Y. *Int. J. Hyperthermia,* **2002**, *18,* 194.
[112] Ito, A.; Tanaka, K.; Honda, H.; Abe, S.; Yamaguchi, H.; Kobayashi, T. *J. Biosci. Bioeng.*, **2003**, *96*, 364.
[113] Jordan, A.; Rheinl, T.; Waldofner, N.; Scholz, R. *J. Nanoparticle Res.,* **2003**, *5*, 597.
[114] Hilger, I.; Fruhauf, K.; Andra, W.; Hiergeist, R.; Hergt, R.; Kaiser, W.A. *Acad. Radiol.,* **2002**, *9*, 198.
[115] Jones, S.K.; Winter, J.G. *Phys. Med. Biol.,* **2001**, *46*, 385.
[116] Ma, M.; Wu, Y.; Zhou, J.; Sun, Y.; Zhang, Y.; Gu, N. *J. Magn. Magn. Mater.,* **2004**, *268* 33–39.
[117] International Committee on Nonionizing Radiation Protection (ICNIRP) *"Guidelines for Limiting Exposure to Time-Varying Electric, Magnetic, and Electromagnetic Fields (up to 300 GHz)." Health Physics,* **1998**, *74*, 494.
[118] Li, G.C.; Mivechi, N.F.; Weitzel, G. *Int. J. Hyperthermia*, **1995**, *11,* 459.
[119] Ito, A.; Tanaka, K.; Kondo, K.; Shinkai, M.; Honda, H.; Matsumoto, K.; Saida, T.; Kobayashi, T. *Cancer Sci.*, **2003**, *94*, 308.
[120] Gordon, R. T.; Hines, J. R.; Gordon, D. *Med. Hypothesis*, **1979**, *5*, 83.
[121] Yanase, M.; Shinkai, M.; Honda, H.; Wakabayashi, T.; Yoshida, J.; Kobayashi, T. *Jpn. J. Cancer Res.,* **1997**, *88*, 630.
[122] Yanase, M.; Shinkai, M.; Honda, H.; Wakabayashi, T.; Yoshida, J.; Kobayashi, T. *Jpn. J. Cancer Res.*, **1998**, *89*,463.
[123] Shinkai, M. *J. Biosci. Bioeng.*, **2002**, *94*, 606.
[124] Jordan, A.; Scholz, R.; Wust, P.; Fahling, H.; Krause, Wlodarczyk W.; Sander, B.; Vogl, T. *Int. J. Hyperthermia,* **1997**, *13*, 587.
[125] Hilger, I.; Hiergeist, R.; Hergt, R.; Winnefeld, K.; Schubert, H.; Kaiser, W.A. *Invest. Radiol.*, **2002**, *37*, 580.
[126] Gneveckow, U.; Jordan, A.; Scholz, R.; Brüß, V.; Ricke, J.; Feussner, A.; Rau, B.; Wust, P. *Med. Phys.*, **2004**, *31*, 1444.

Received: February 22, 2007 Revised: June 12, 2007 Accepted: June 23, 2007